The Development of an Analytical Model of the Transport Phenomena between Two Fluids in a Microchannel with an Application to Amino Acid Detection

A Dissertation

Presented in Partial Fulfillment of the Requirements for the

Degree of Doctorate of Philosophy

with a

Major in Mechanical Engineering

in the

College of Graduate Studies

University of Idaho

by

Jennifer Lee Hasenoehrl

Major Professor: Steve Penoncello, Ph.D.

Committee Members: John Crepeau, Ph.D.; Jacob Leachman, Ph.D.; Tao Xing, Ph.D.

Department Administrator: Steve Beyerlein, Ph.D.

August 2016

Authorization to Submit Dissertation

This dissertation of Jennifer Hasenoehrl, submitted for the degree of Doctorate of Philosophy with a Major in Mechanical Engineering and titled "The Development of an Analytical Model of the Transport Phenomena between Two Fluids in a Microchannel with an Application to Amino Acid Detection," has been reviewed in final form. Permission, as indicated by the signatures and dates below, is now granted to submit final copies to the College of Graduate Studies for approval.

Major Professor: _____ Date: _____

Steve Penoncello, Ph.D.

Committee Members: _____ Date: _____

John Crepeau, Ph.D.

_____ Date: _____

Jacob Leachman, Ph.D.

_____ Date: _____

Tao Xing, Ph.D.

Department Administrator: _____ Date: _____

Steve Beyerlein, Ph.D.

Abstract

A transport model for the fluid flow of two immiscible fluids in a microchannel is presented. The fluids, water and acetone, are at a Reynolds number of less than 10 to ensure laminar flow during the diffusion portion of the microchannel. Laminar flow provides the means of diffusion of molecules to occur between the fluids without the fluids mixing all while in a microdevice. In this research, amino acids and fluorescamine are carried by the water and acetone, respectively.

The fluid properties as carriers of the molecules are unknown for transport phenomena calculations so best predictions are calculated from diffusion theory and Einstein's diffusion equation. The diffusion coefficient for fluorescamine (1.77×10^{-6} cm^2/s in acetone and 6.11×10^{-7} cm^2/s in water at 298 K) is compared to the calculated versus manufacturer provided data for fluorescein, a similar fluorophore that gives off light at a differing wavelength.

Thermal effects on the fluids as well as chemical reactions are investigated. The model is validated with experimental results from the literature and experimental measurements taken in lab of fluorescing beads in moving water. Comparison between the model results and literature show an agreement within 10%. This can be attributed to diffusion coefficients and temperature differences within the model. The model predicts diffusion of fluorescamine-tagged amino acids to the acetone side by 1.88 mm of the channel length.

Acknowledgements

I appreciate the guidance and mentoring of Dr. Steve Penoncello. Steve, my education far surpassed what the shelves in an engineering library could ever hold, and I would not have lasted as long as I did without your support and encouragement. I am even more grateful for you letting me spread my wings and continuing to work with me when I landed in Pasadena of all places.

I thank my committee members, Dr. Jake Leachman, Dr. Tao Xing and Dr. John Crepeau. Your cooperation and support for a long-distance research experience was fabulous and much appreciated.

I am thankful for funding support from the Dr. Richard B. Stewart Thermal Fluid Sciences and Walter B. Hayes Engineering scholarship funds, the Society of Women Engineers scholarship, the Idaho Waters of the West GK-12 program in conjunction with the National Science Foundation, and the Idaho Space Grant Consortium for internships and fellowships.

This work described in this dissertation was performed at the University of Idaho sponsored by the Idaho Space Grant Consortium. Publication support was provided by the Jet Propulsion Laboratory, California Institute of Technology, under a contract with National Aeronautics and Space Administration. I thank Stewart Sherrit, Aaron Noell, Anita Fisher, Nobuyuki Takano, Michael Lee and Andrew Aubrey for allowing my participation in the AstroBioNibbler task. I also thank Yosi Bar-Cohen, Randy Foehner, Josh St. Vaughn, Kobie Boykins, Lori Shiraishi, Curt Henry and Melora Larson for allowing me to stay at JPL for the duration of my dissertation. Lastly, I thank Cami Vongsouthy, Karen Moran and fellow members of Section 516 for their support while I finished writing.

Dedication

This path has not always been easy, but it has taken me to many great places, and during this journey, I have been lucky mostly thanks to the following people:

To Steve—for a true dedication in seeing your student through. Thank you!

To my parents, Shawn and Karen—thanks for encouraging me to pursue my dreams, even when it felt like I might not reach them. Thanks for being my loudest cheerleaders and letting me stretch my wings. Thanks for the care packages and stickered envelopes filling the mailbox and answering late night calls after a long day far from home.

To my little sisters, Sara, Andrea, Lauren and Kalyn—thanks for being wise beyond your years. Thanks for pushing me and for the reminder "older" simply means a difference in age.

To my friends and mentors—thanks for the guidance and nurturing as I grew in my personal life as well as my professional life. A special thank you to my furry friends for keeping my feet and spirit warm as I worked. Thank you Veronica, Lisa, Jamie and Ola.

To the people I met while at the University of Idaho, friends, classmates, cohort members, students, instructors and faculty—while silver and gold unite us always, go Vandals!

To the people I met while at the Jet Propulsion Laboratory—thanks for helping me feel like I belonged and for giving me a place to experience the wonders of the universe in a different way than watching meteor showers from a trampoline in a backyard in Idaho. A special thank you to Karla for helping to align the galaxy in more ways than one.

To those who will endeavor in the footsteps of engineers before you—shoot for the stars. A backup plan does not need to exist for missing the moon.

To Chris—thanks for your patience, support and help with coding. Perfect timing!

To my family—work hard, play hard, and love with all your heart, forever and for always.

Table of Contents

List of Figures

List of Tables

List of Equations

List of Symbols

A	adsorption ratio [-]
b	half width [micron]
C	concentration [-]
D	diffusion coefficient [-]
d	depth of channel [micron]
F	external body force [N]
f	substitution factor [-]
G	stability value [-]
L	length of channel [m]
m	mass flow rate [kg/s]
P	pressure [kPa]
Pr	Prandtl number [-]
Q	volumetric flow rate [m^3/s]
R	gas constant, 8.31447 [J/mol-K]
r	radius of molecule [micron]
Re	Reynolds number [-]
S	resistance value [-]
T	temperature [K]
u	velocity [m/s]
W	volume to surface area ratio [-]
w	depth of channel [micron]
x	width of channel [micron]

Greek letters:

Δ	difference [-]
μ	viscosity, kinematic [cm^2/s]
η	viscosity, dynamic [$N\text{-}s/m^2$]
τ	stress, shear [N/m^2]
ν	viscosity, kinematic [m^2/s]
ω	volumetric flow rate [m^3/s]

Superscripts:

I	designation of fluid 1
II	designation of fluid 2
n	time step [s]

Subscripts:

E	entrance length [micron]
i	spatial step [micron]
R	ratio
thick	fluid with higher viscosity value
thin	fluid with lower viscosity value
x	direction along width
y	direction along length
z	direction along depth

Chapter 1: Introduction

One of the objectives of NASA's Astrobiology Program [1] is to develop new technologies to improve scientific understanding of life in our solar system. This program funds research to help answer questions regarding how life began and evolved, how life can be detected beyond Earth, and what may be next for life in the universe. To help answer how life can be detected beyond Earth, the AstroBioNibbler (ABN) task was selected to develop an instrument capable for a flight mission to Mars to detect signs of life as indicated by the presence of amino acids [2].

Purpose of the ABN:

The ABN is a task proposing an in-situ instrument designed to detect and quantify amino acids present within a collected soil sample. Astrobiologists consider amino acids the "building blocks of life," and their presence can signify extant or extinct life [1]. The focus of the ABN, however, is to develop microscale sample extraction and detection capabilities. Current Earth-based laboratory technologies are large and heavy, and neither characteristic is ideal for space exploration. By using a microdevice as the in-situ instrument, small amounts of sample would be needed, and the probability of selection on a future mission increases with a smaller footprint, lower power needs and reliable reusability.

The path of an amino acid through the ABN:

The ABN builds on existing technologies of microfluidic separation and subcritical water extraction for capturing and quantifying amino acids from a soil sample. These

processes will take place in microchannel networks on four-inch diameter borofloat glass wafers (also called chips); the glass acts as the material substrate and structure for this instrument. Figure 1 provides a system map for key inputs and components including processes and outputs contained on this chip.

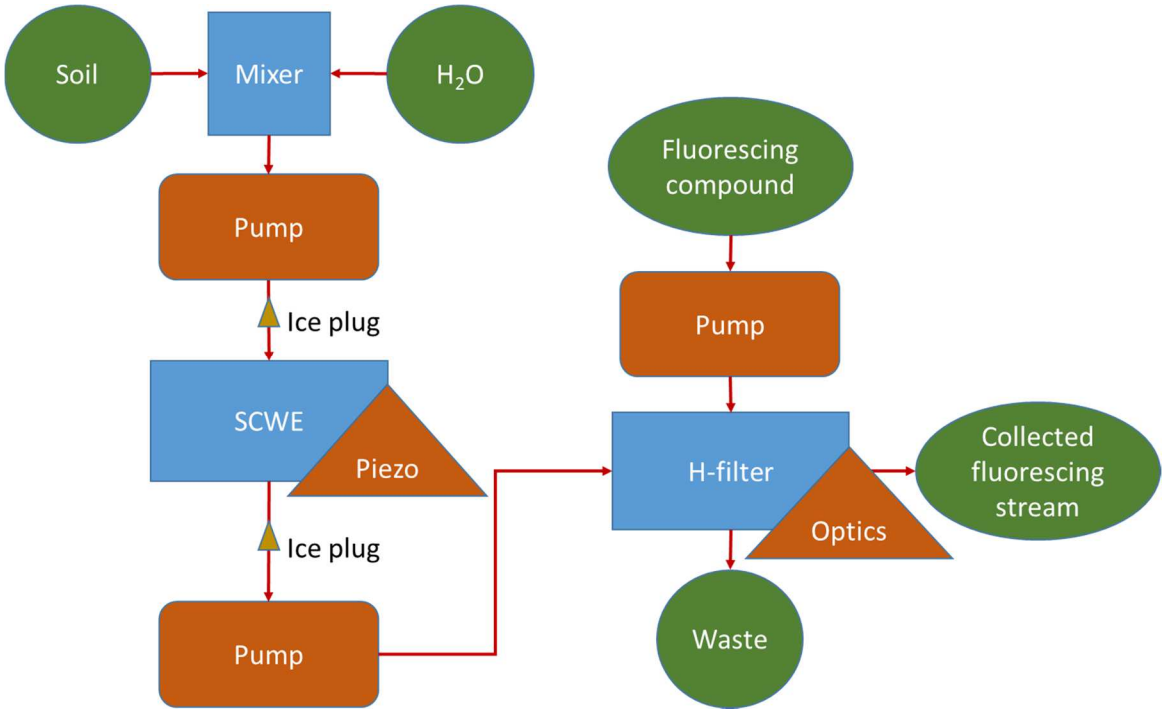

Figure 1. System map of sample handling and detection system. Input/output streams are in green circles. Processes are in boxes with blue representing sample processing and orange representing manipulation/detection instruments requiring power; the overlapping orange triangles occur on chip. The noted ice plugs (as small gold triangles) hold the sample in place while extraction occurs.

This system map shows the progression of the soil sample from the top left to the product of the tagged and collected amino acid chains in the fluorescing stream at the right of Figure 1.

The soil and water are mixed so any potential organic contents within the soil can be transported along with the suspended soil particles in a fluid stream through the rest of the chip. The subcritical water extraction (SCWE) portion of the chip prepares this soil suspension for its future processing prior to the mixture entering the H-filter portion of the system. At the H-filter, the suspended soil sample can interact through localized diffusion

with a fluorescing compound. The H-filter is a unique design, explained in more detail in Chapter 2, which allows for two fluid streams to flow adjacent to one another at low Reynolds numbers. This arrangement permits the fluids to remain separate, but molecules can diffuse across what is called a laminar flow diffusion interface (LFDI), the boundary between two adjacent fluid streams. The fluorescing compound from the reactant stream tags amino acids from the sample stream. These tagged amino acids are collected in the reactant stream where optics near the exit of the H-filter can detect and quantify the strength of the fluorescence. The exit streams can be collected and concentrated, or dumped depending on the requirements of the mission.

Specifics of the amino acid pathway:

Once the soil is captured and delivered from sampling instruments as 150-micron diameter particles, it will be mixed with water to suspend and possibly dissolve broken chains of amino acids. This mixture is transported to the SCWE chamber, a circular, empty space with a piezoelectric disc attached to the outside of the glass in order to provide heating and agitation as roughly sketched in Figure 2.

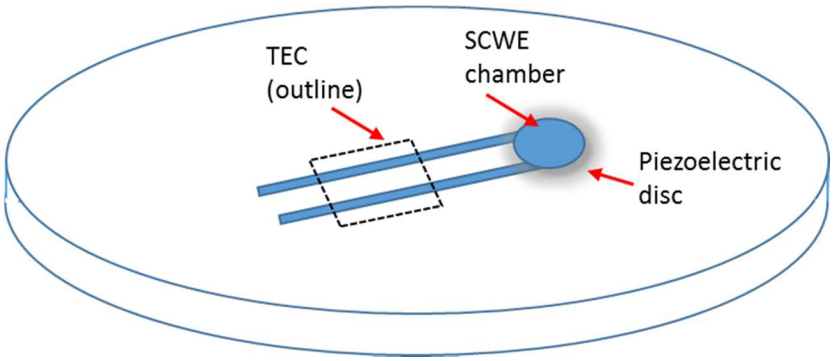

Figure 2. SCWE chamber on glass wafer with footprint of the thermoelectric cooler (TEC) to create frozen plugs in channel and the piezoelectric disc to create resonance and heating.

The goal of this part of the system is to heat water to a specific subcritical temperature in order to dissolve or break down amino acids from the larger soil particles without vaporizing the water. Ice plugs are created in the channels leading to and from this chamber by thermoelectric coolers in order to hold a sample of a desired size in an enclosed volume where the pressure helps the water to reach higher-than-atmospheric temperatures without boiling. The goal is to heat within the 150-200°C range without a phase change occurring; therefore, increased pressure to the system must be maintainable. Figure 3 shows the vapor pressure of water, which is the main consideration for the SCWE operational parameters. The water begins at room temperature and pressure, and an estimated ending state is shown.

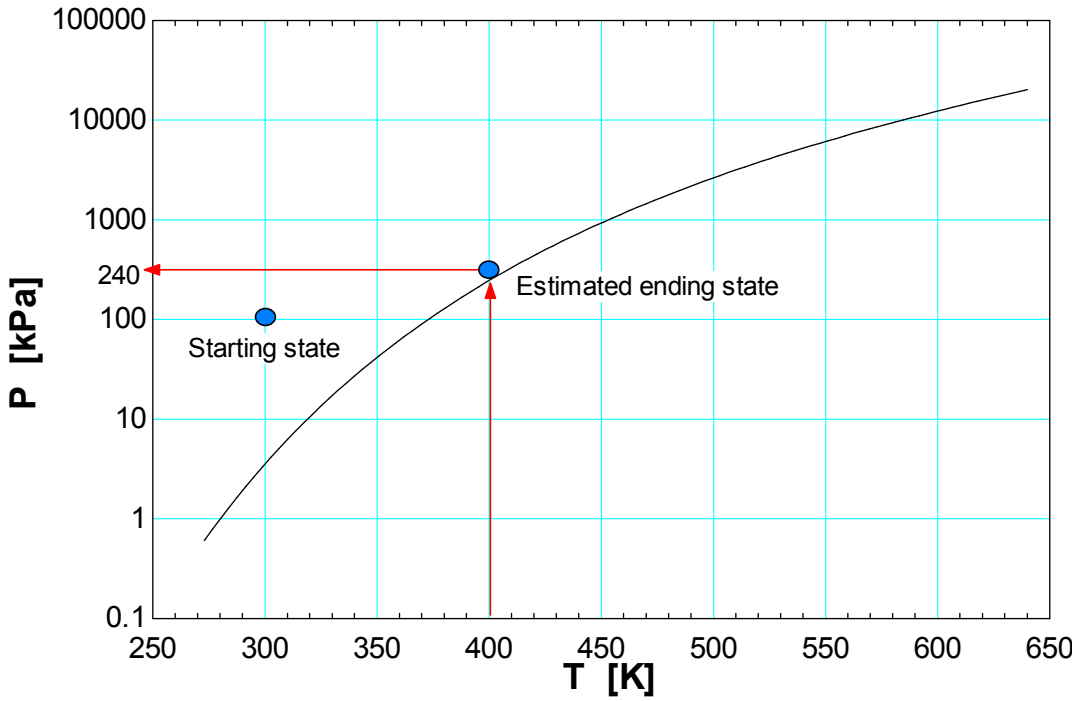

Figure 3. Vapor pressure of water from 0°C to the critical point. Starting and ending states of the SCWE process are depicted as blue dots. Plotted in EES from equation of state [3].

Once the water reaches the desired temperature, the coolers are shut off to melt the temporary ice plugs, and the soil slurry is emptied from the SCWE chamber. Two possibilities to proceed include settling out the large particles. Without large particles, the

possibility of clogging the H-filter portion of the system is minimized. The second possibility is to push the soil slurry through the H-filter but keep soil particles suspended using a resonance frequency produced by piezoelectric discs.

Preliminary experiments use a pump to move 10%-by-weight soil slurry from an agitator cup (a cylindrical container that has a line out to a pump and a piezoelectric disc as the bottom of the cup for mixing and suspension purposes). Connections between the chips and the pumps are nanoports. Figure 4 shows the nanoports that have been epoxied to the inlets and outlets on chip. The nanoports work much like a Swagelok fitting in that they tighten down on the tubing as the nanoport cap is twisted onto its base.

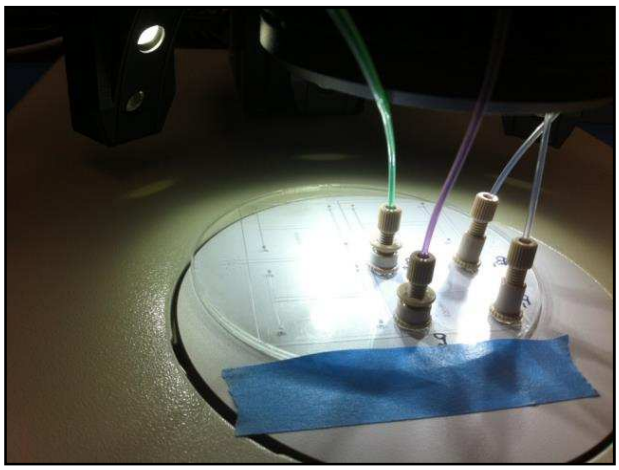

Figure 4. Nanoports with input lines (green and purple) on the left and output lines (look clear) on the right during proof-of-concept experimentation at JPL [4].

The colored tubes in Figure 4 contain water with food dye to observe whether the streams in the channel mix as explained next.

Fluid flow through microchannels is investigated with two laminar streams of fluid flowing alongside each other in an H-filter as depicted in Figure 5.

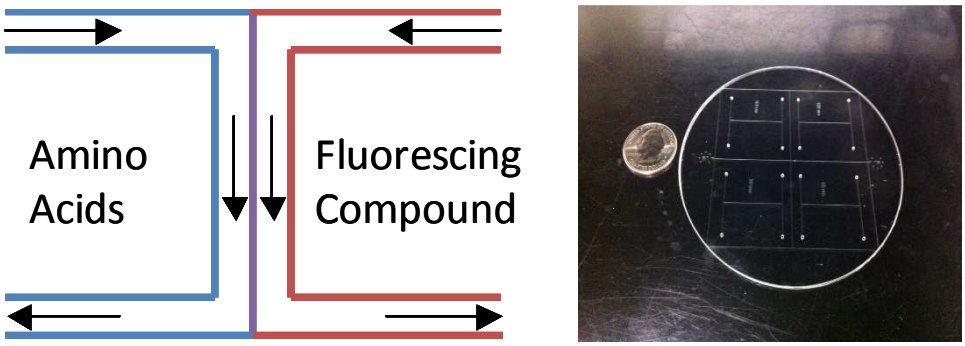

Figure 5. Diagram of H-filter (left) and photo of fabrication prototype manufactured at JPL (right) displaying four H-filters with different aspect ratios of the diffusion channel width/height. Diagram's left side (blue) contains water with sampled material, right side (red) contains fluorescing compound, and mixing at centerline (purple) occurs slowly since fluid streams experience laminar flow [5].

One stream is an aqueous soil solution containing amino acids; the other stream contains a high concentration of molecules that fluoresce when bound with amino acids [4]. At the end of the H-filter, the concentration of the diffused amino acids bound to the fluorescing compound is measured using optical detection of the fluorescent signature.

The optical detection is a camera on a rail that can move along the width of the channel. The placement of this camera along the length of the H-filter must be considered carefully. While placing the camera too far upstream means the molecules will not have sufficient time to diffuse to the appropriate stream, if the camera is placed too downstream, the molecules may have diffused too much. Photo bleaching may occur where the fluorescence is too strong to detect the locations of minimum and maximum levels across the width of the channel. It is possible the prototype chip shown in Figure 5 will not have a long enough diffusion channel. To solve this, a very long H-filter was etched as shown in Figure 6.

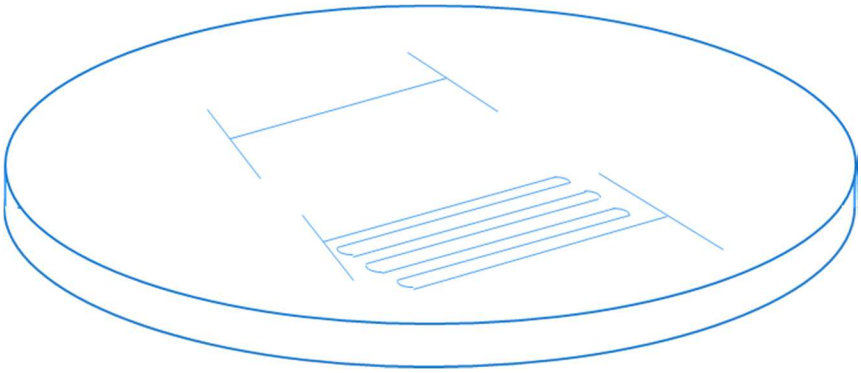

Figure 6. Original and modified H-filter configurations.

The idea behind the longer, meandering H-filter is to allow for more time for diffusion to occur if the flow rates must be on the higher end of the range (flow rates have ranged between 1 and 100 microliters per minute in proof-of-concept experiments). The slower the flow, the more chances for the molecules in the streams to begin to diffuse into one homogenous stream from a diffused molecule standpoint. The faster the flow, the less likely enough diffusion can take place before the fluid streams reach their exit points. Due to these constraints, H-filter length and layout as well as resident time are critical parameters.

Considerations for amino acid detection:

Device configuration and operational parameters can be determined through a best-guess experimental procedure. By using theory, CFD and building on previous designs from literature, an optimal device can be tailored rather than relying on the guess-and-check routine that was once typical for these microdevices. In this work, modeling of the fluid flow and the diffusion between the streams is presented. The mass transfer between the streams may be affected by a variety of the molecular properties including type of molecules and their molecular size, shape and mass, physical properties such as temperature, pressure, resulting coefficients of diffusion and viscosity, fluid flow rates, and geometric properties

such as the microchannel length, height and width [6-8]. Created models are compared to data from the literature as well as experimental data. These models of the fluid interaction and flow can also guide design iterations and fabrication procedures of the H-filter as new needs are introduced.

The use of computational fluid dynamics (CFD) software with the incorporation of particles in the flow and heat transfer to the fluids adds to the current state of the art for laminar fluid flow of adjacent streams in microchannels. Particles are generally difficult to move as a fluid. The additional constraint for them to be inside a reusable microdevice presents a challenge. The operational range of temperatures may also influence diffusion and reaction rates and must be considered.

Some design limitations include a targeted weight limit of 1 kg. Since orientation of the device may vary, rectangular channels with the smallest dimension at three times the diameter of the largest suspended soil particles would be ideal so that gravity effects will not pose a risk to the operation of the system based on an altered orientation.

Chapter 2 reviews current state of the art within the literature. It is broken into subsections for a detailed investigation into the theory of low Reynolds number flows, microdevices, uniqueness of the application and design considerations for Mars, effects of particles within the flow, and heat transfer effects. The theory of corresponding states is also reviewed; few data are available for diffusion coefficients and chemical reactions between the fluorescing agent and amino acids with water and acetone as the working fluids. Chapter 3 outlines the fluid model through a given geometry with diffusion between the fluid streams, and Chapter 4 expands the model to include heat effects with chemical reactions. Chapter 5 provides validation for the models presented. This occurs by comparing finite

difference solutions to CFD solutions and experimental work. Chapter 6 concludes the current and presented work while Chapter 7 proposes future work and possible directions in which to continue efforts. Details regarding the modeling can be found in the appendices as well as reference material.

Chapter 2: Literature Review

While this dissertation focuses on fluid dynamics at small scales, the use of low Reynolds number flow theory provides the basis of the modeling work and argues the feasibility of using a microfluidic device to detect amino acids with heat transfer and geometric constraints. Microdevices, and their characteristics and history within fluidics are reviewed. The application considerations are summarized.

The microdevice world has expanded rapidly with the aid of computer modeling and precision machining. Conversely, as pointed out by Livak-Dahl et al. [9], microfluidics has expanded the field of science and engineering for their easy incorporation with other devices and their need for a small amount of fluid. As fluidic systems are miniaturized, volumetric flow rate and gravity effects are reduced but the diffusive rates and driving pressure are increased.

Theory of low Reynolds number flows:

The Reynolds number is used to indicate whether a flow may be laminar or turbulent. It is calculated as a ratio of inertial to viscous effects within a flowing fluid as shown below

$$Re = \frac{\rho u L}{\mu} = \frac{uL}{\upsilon} = \frac{\text{inertial forces}}{\text{viscous forces}} \quad (1)$$

where the product of the density (ρ), velocity (u) and length (L) are divided by the dynamic viscosity (μ). (Kinematic viscosity, ν, can also be substituted for the ratio of dynamic viscosity, μ, to density, ρ.) When the inertial effects are very small in comparison to the

viscous effects and can essentially be ignored, the Reynolds number is also small. This is the case for the ABN.

Though the laminar-turbulent transition occurs near a Reynolds number of 2300 for internal flow, a low Reynolds number flow is considered by most researchers to be any value below one in a regime where turbulence does not occur [10]. A lecture by Purcell [11] normalizes examples to a Reynolds number of one and shows that for a body to move, a force (F) acting upon that body must be equal to the square of the dynamic viscosity (μ) of a fluid divided by the fluid density (ρ) as shown below.

$$F = \frac{\mu^2}{\rho} \tag{2}$$

As Purcell [11] points out, particles moving in low Reynolds flow cannot simply drift. The fluid around them has to move too, which also means that the force defined above will tow anything with a Reynolds number of one. Therefore, any stirring that may take place will not cause separation or mixing; the surrounding fluid is moved along with any molecules or particles within the flow. Any description of low flow rates with respect to the molecules and particles will then be characterized by the bulk fluid movement. Momentum (Navier-Stokes) equations reduce to

$$-\nabla p + \mu \nabla^2 \vec{u} = 0 \tag{3}$$

which is known as Stokes flow. The flow becomes steady, and velocity changes with time are no longer present.

At the same time, operational barriers occur near this unity value. Surface tension can be a major force on the fluid even if turbulence does not occur at low Reynolds numbers [12]. Surface tension effects would be present at the start/stop of a flow and at transitions

between chips and reservoirs where a pump would have to overcome this force to begin to flow fluid through empty lines and channels.

Despite concerns of starting fluid movement, the largest advantage of microchannels with small amounts of fluid moving slowly enough their Reynolds numbers are near unity is the way that the fluids do not mix due to turbulence, rather that "mixing" occurs only on a molecular level through diffusion. Various research groups have used this knowledge to enhance mixing by staying away from low Reynolds numbers [13, 14]. Conversely, diffusion-only mixing is advantageous in developing a device that can separate molecules and particles without mixing the fluid streams, which would work well for many detection and separation applications including the needs of the ABN. If the ABN also wishes to concentrate the separated molecules, then ratio of the exit stream areas needs to be factored into a design so diffused areas of the channel are collected appropriately.

Laminar Flow Diffusion Interface (LFDI):

The LFDI is found only where fluids are under low Reynolds flow conditions. The fluids can flow alongside one another while not mixing; mixing usually occurs due to eddies from flow interference and turbulence generated in the flow stream. These interfaces exist where the streams interact. Therefore, if three streams are present, two LFDIs will be present.

The shear stresses within the adjacent immiscible flows match at the interface between the fluids as well as their velocities [15]. The following, Equations 4-6 for sheer and velocity profiles, are for two fluids that each take up half the channel flow volume.

$$\tau_{xz} = \frac{(p_O - p_L)b}{L}\left[\left(\frac{x}{b}\right) - \frac{1}{2}\left(\frac{\mu^I - \mu^{II}}{\mu^I + \mu^{II}}\right)\right] \quad (4)$$

$$u_z^I = \frac{(p_O - p_L)b^2}{2\mu^I L}\left[\left(\frac{2\mu^I x}{\mu^I + \mu^{II}}\right) + \left(\frac{\mu^I - \mu^{II}}{\mu^I + \mu^{II}}\right)\left(\frac{x}{b}\right) - \left(\frac{x}{b}\right)^2\right] \quad (5)$$

$$u_z^{II} = \frac{(p_O - p_L)b^2}{2\mu^{II} L}\left[\left(\frac{2\mu^{II} x}{\mu^I + \mu^{II}}\right) + \left(\frac{\mu^I - \mu^{II}}{\mu^I + \mu^{II}}\right)\left(\frac{x}{b}\right) - \left(\frac{x}{b}\right)^2\right] \quad (6)$$

The viscosities are denoted with I and II for the fluid they represent, and the starting and ending pressures are labeled with 0 and L for the pressures at the entrance and exit of the diffusion channel, respectively. Li and Renardy [16] work through two immiscible liquids at low Reynolds flow. Their study focuses on droplets within the fluid, and how those droplets can stretch or break apart in the flow because of differing viscosities. Finlayson [17] presents an analytical solution of two immiscible fluids where the velocity matches at the interface between the two fluids.

Williams et al. [18] used SPLITT (split flow thin-cell) fractionation to help separate wanted and undesired particles between two fluids. Instead of a physical barrier or fluids of differing viscosities, streams of the same fluid are flowed side-by-side, and the particles within these streams are separated by density due to settling. It is pointed out here that the LFDI acts like a virtual membrane between fluids and emphasize the importance of acceptable limits in which settling can and will occur.

Schattka et al. [19] use the LFDI to precondition samples. Their work develops a model for flow thicknesses. This way, the “filtered” stream can be split off at the end of the diffusion channel. Experimental procedures discarded the first 90 microliters of fluid through the channel (equivalent to three full channel volumes) to allow diffusion to equilibrate.

Similarly, Mansfield et al. [20] prepare samples using a LFDI so wanted components of the flow can be collected and concentrated for further analysis. The major difference between their work and the proposed work for this dissertation is their use of capillary forces to draw the fluid through the microchannels whereas a pump will move the fluid in the microchannels of the ABN.

Jandik et al. [21] use an H-filter to take advantage of the LFDI for sample preparation. The fluids were moved by external syringe pumps through a network of multilayered microchannels, and although whole blood was used, fouling was overcome by using saline as the receiving fluid. Nelson et al. [22] and Foley et al. [23] use a LFDI to model and measure diffusion between channels as well. Kuo and Chiu [24] present mass transport control in microfluidic devices, specifically with a focus on the LFDI. The segmenting of fluid droplets within another fluid can minimize the diffusion between the two fluids. Conversely, the act of increasing the diffusion interface between the two fluid flows while in the diffusion channel together will increase the diffusion rates. This can be done by folding the stream onto itself, providing rough channel walls and narrowing the channel width/depth.

Not all of the time does the LFDI reside along the centerline of the diffusion channel. The ratio of the flow volume used by each fluid is a function of their inlet pressure and viscosity. An example of how this might differ is shown in Figure 7.

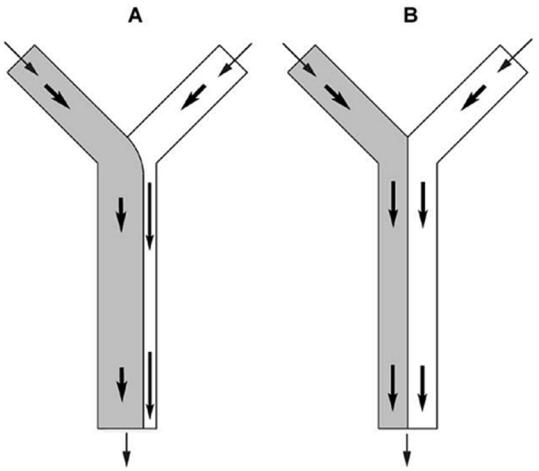

Figure 7. Results from Hatch et al. [25] where viscosity values influence the flow characteristics.

The fluids do not have the same viscosity even though they have the same inlet flow rate. The portion of the channel is influenced by this fluid property. Kuczenski et al. [26] use feedback to the pressure control system to adjust the fraction of the channel one specific side the fluid is taking up. While the viscosity and pressure influence the volumetric flow, the diffusion coefficient is used to help predict location during molecular diffusion as shown by Equation 7. The diffusion coefficient can be calculated based on its temperature dependence as shown below [27].

$$D_{AB} = \frac{RT}{6\pi\mu_B r_A} \tag{7}$$

The Stokes-Einstein equation can provide a good estimate of the diffusion coefficient for an unknown molecule even if the molecule is not spherical.

An alternative to flowing is to allow the amino acids to mix with the fluorescamine prior to passing through the diffusion channel. In this case, the channel would be used to "sort" the molecules based on size in the way modeled by Hatch et al. [25]. The problem would be whether fluorescamine binds with the fluid molecules and not the amino acids present. This would give a false positive as indicated by the strength of fluorescence.

Kamholz and Yager [28] summarize the scaling of the Einstein diffusion approximation where diffusion displacement is estimated during stopped flow. Once flow begins, the velocity profile becomes non-uniform, and their modeling predicts diffusion occurring more rapidly at the no-slip boundary as shown in Figure 8.

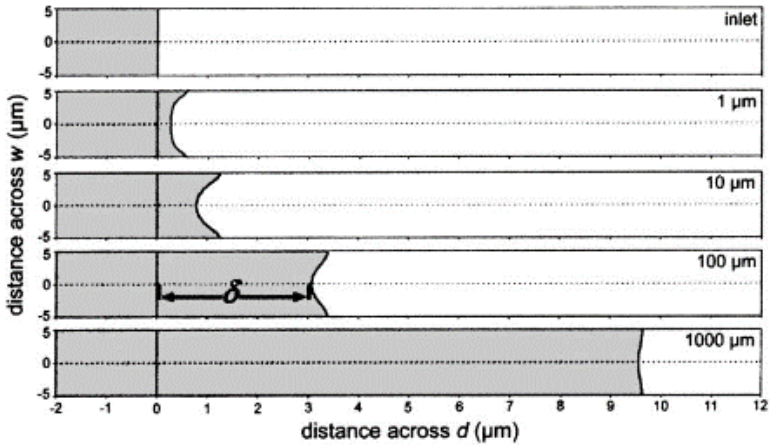

Figure 8. Channel visualizations for diffusion across the channel width and depth according to Kamholz and Yager [28] where each slice represents a specified length downstream from or at the inlet.

Hatch et al. [25] warn of errors with a one-dimensional analysis. Whether relevant or not, multidimensional analysis could include convection and binding reactions present in the flow which may not be visible from one dimension. Premixing diffusion-based analysis is first reported by Hatch's team. The fluorescein and bovine serum albumin (BSA) were allowed to react prior to entering the diffusion channel in a T-sensor. Buffer flowed on the other side of the channel and diffusion of the tagged molecules happened over the length of the channel. Later experiments added glycerol to the buffer to match viscosities of the two fluids. Doing this allows a one-dimensional model to be valid since residence times of both fluids are similar or equal.

Hatch et al. [25] also used hydrogels to form a mechanically stable interface at the surface of the fluid sample to preserve samples and reagents. This method cannot be used more than once since the hydrogels line the channels and are consumed by the flowing fluids. The use of hydrogels is not a preferred method of detection for the ABN because of the limits on size and quantity of detectors.

Bowden et al. [29] extracted hydrocarbons from oil. They etched microscope slides to fabricate H-filters for testing hexane and oil with residence times of less than 5 seconds. With diffusion of species across the LFDI between two liquids, scaling effects are noted by Figure 9 where Ismagilov et al. [30] experimentally verified the model with x-ray photography.

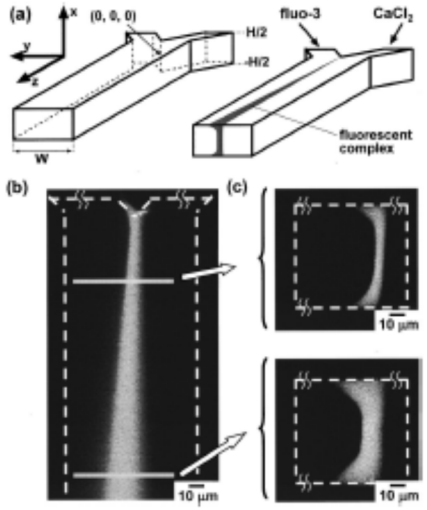

Figure 9. Effects at walls along length of channel [30].

Kashid et al. [31] used slug flow to investigate mass transfer with CFD modeling. Their assumptions simplified the modeling to transfer at the boundaries of the slugs. Their model included a chemical reaction between species, which is an important consideration with the model presented in this dissertation. As the chemical species move, they react with

each other and the fluids they encounter from a chemistry standpoint, not a momentum reaction.

According to Brody et al. [12], the extraction within microfluidic systems is best controlled while Re<<1 else mixing in addition to diffusion may occur at Re>>10. Their experiments show the diffusion of 0.5-micron diameter fluorescent beads between two fluid streams at a rate of 100 μm/s. It is also noted that the entrance length of the flow is half the diameter of the channel, which is quite small in comparison to the overall channel length.

Theoretical development of the movement within the microfluidic channel is modelled by Kamholz and Yager [32]. Their model uses BSA, a blood serum with proteins. Since T-sensors are commonly used to measure diffusion coefficients, they compare tagged proteins to theoretical models. The fluorescence measurements follow an error function as predicted by analytical calculations.

Microdevices:

Two types of sensors in this microfluidic total analytical system (μ-TAS), also referred to as microdevices, are T-sensors and H-filters. Each has at least two inlet streams of fluids, usually with different properties including the type of fluid or the types of molecules suspended or dissolved within the fluid. Weigl and Yager [33] define the characteristics of these systems and describe how all analytical functions can be performed by this one system. They argue that separation of particles is the most difficult part of this system since centrifugation and filtering are poor options at this microscale.

It is also pointed out that although many functions can be performed on a chip such as sampling, separation, dilution, reactions and detection among others, by 1999, a single

chip had not been fabricated to perform all of these functions on one device. The microdevices allow for diffusion without fluids mixing if they flow at laminar conditions for their channel size. A bonus for these microdevices is their ability to sort particles by size through diffusion. The T-sensor was the first to perform both separation and detection in the same device, and the smaller the molecules are for the diffusion, the faster they will move between the streams [33].

Kamholz et al. [34] analyze a T-sensor; these sensors can only be used for separation and detection within the channel as the output stream is a single outlet. This would be satisfactory if the analysis takes place prior to the fluids leaving the channel. In the event that the fluid is recirculated for concentrating, having the tagged sample separate from the reacted stream at the exit would be ideal. Silicon devices with photoresist etching were bonded to Pyrex glass wafers for the structural component. The fluid is albumin, and a "butterfly effect" is mentioned for the flow nearest the channel walls where diffusion occurs more rapidly due to resident times of a non-uniform velocity profile.

Stone et al. [35] review microdevice uses and unique design aspects. Devices are considered "microfluidic" when fluid flows are controlled or manipulated at a millimeter or less. Forces driving microfluidic flows include pressure gradients in pipe flow and capillary effects with surface tension changes. Other driving forces include electric fields, magnetic fields, sound and rotation. Though acoustic streaming might help with particle settling, there will not be any acoustic energy used for particle suspension for the ABN as the fluid travels

through the diffusion channel. Electric and magnetic fields will also be ignored, and rotation effects are not present since the channel is not curved.

Using the principles described previously, microchannel devices are becoming common for extraction, detection and interaction of organic molecules in chemical and biological applications. Mixing or separation of fluid streams and the diffusion of specific molecules play a large role in the design and fabrication goals of these devices. The network of microchannels is most commonly etched on a glass or composite wafer. Devices are generally small in footprint and can be made economically so that they can be one-use devices to minimize the risk of cross-contamination between samples.

Microdevices benefitted from the addition of the MEMS (micro electrical mechanical systems) discipline to the field of engineering. The microchannel design with laminar adjacent flow of two liquids has been studied since the early 1990s. Most recently, it has been used as a medical device for quick blood testing. The medical industry is looking to use such devices as a way to test for specific diseases or conditions with a small amount of body fluid. Due to the total volume of fluid space within these devices, only a few drops of blood, urine or saliva are needed, and the results are quick if a chemical indicator is used. They can be made to be inexpensive so one-and-done does not cross-contaminate sample results. The difference with the ABN is the need for it to be reliably reusable or definitively disposable.

Microdevices were established as a way to move and manipulate small amounts of fluid. External components can induce bulk fluid movement, such as a pump, or chemical species transport in the way that electrophoresis can manipulate specific ions within the bulk fluid. Microdevices for separation and detection of fluid components began as T-sensors. In

these devices, there are two inlets of two separate fluids and the detection occurs while the fluids are still passing through the detection portion of the channel. The outlet (waste) streams do not matter so all fluid exits from one outlet. H-filters are very similar, but the outlet streams are separate and can be collected for analysis post-channel.

SPLITT devices are also referenced in literature where separation can be obtained through the application of an electric field to the fluid channel, such as electrophoresis. While this may be attractive, the development of the ABN will be based on diffusion for amino acid detection.

Work prior to the ABN includes work by other JPL research teams to use Earth-based detection systems for proof-of-concept amino acid detection in the Atacama Desert. Skelley et al. [36] developed a capillary electrophoresis instrument where an external electrical field and pneumatic pumps were capable of detecting amino acids at 70 parts per trillion to 100 parts per billion from soil in the Atacama Desert. The chip with the microchannel network had a small footprint yet the external equipment for the detection and fluid manipulation, though portable, was large in comparison to the chip. It is common for microdevices to use electrophoresis to separate polar molecules to specific locations within the stream. Other microdevices currently separating molecules effectively rely on an external electric field to push or pull molecules through electrophoresis. This adds complexity and overall weight that could limit where the ABN is sent.

Kapoor et al. [37] studied biomolecular reactions in Poiseuille flow. The experimental setup included a glass tube with an inner radius of 0.95 mm. Experiments showed that velocities varied greatly over the cross-sectional area of the tube, and diffusion rates from stopped to moving flow change the concentration quickly.

Some of the earliest microdevices with fluid flow provided chemical analyses for biological samples. The small amount of fluid needed for these devices made them perfect diagnostic tools for detecting specific solutes within the sample. Brody et al. [7] even show it is possible to filter out 16-μm diameter spheres from deionized water. This device differs from later versions in that a LFDI is not used to separate particles across the boundary of two fluids. These researchers do point out potential issues which may arise from surface tension in such small channels, and that even if the channels are wetted, the exit of the channel will still be an issue. Though the purpose of their work was to present an alternative to centrifuging blood samples, their work does not take into account the irregular shape of red blood cells. With a soil sample, it is possible the particles will not be spherical.

Microdevice development began as a way to provide analysis using small amounts of sample. Some of the earliest designs used a permeable membrane to keep the fluids separated yet allow particles to move between the streams [18]. Membranes are prone to fouling so when reusability and ease of cleaning between samples is important, membranes are not preferable. However, the aspect ratio and the direction of diffusion do seem to be important parameters [7, 18].

Experimental and theoretical work regarding the transport of these molecules within the channels takes on several forms, but mainly for medical or geologic purposes. Some devices have specifically been designed to calculate diffusion coefficients of specific solutes by measuring the distance the solutes move from one stream to the next in well-known fluids. The issue with comparing the medical studies to the work of amino acids from a soil sample is that blood is a non-Newtonian fluid, which means the behavior of the fluids within

the microchannel will act differently than water, acetone or other fluids not containing blood components.

Diffusion-based analysis is possible for interactions within the microdevices. Though Weigl et al. [38] focus on passive H-filter systems, they conclude that active systems allow for more precise flow conditions rather than relying on gravity or capillary forces to drive the flow. Channel sizes are bound by the largest particles needing to pass through and keeping the dimensions small enough that the flow remains laminar. Small particles diffuse quickly from one stream to the other. A major disadvantage of passive H-filters is their need to be pressure driven, thus dependent on viscosity, which influences the flow rate and ratio. The pressure changes are proportional to their velocities as shown below [38]

$$U \propto \frac{\Delta P}{\mu} \tag{8}$$

where the pressure drop, ΔP, is experienced equally between the fluid streams along the channel length. The velocities and viscosities are then proportional as shown below [38]

$$\frac{U_{thin}}{U_{thick}} = \frac{\mu_{thin}}{\mu_{thick}} = \mu_R \tag{9}$$

where U is the velocity and μ is the viscosity. The thin and thick describe the width of the fluids within the channel while R is the ratio between them.

The same logic can be applied to solve for the fraction of the volumetric flow taken up by each fluid as shown below [38]

$$\frac{\varpi_{thin}}{\varpi_{thick}+\varpi_{thin}} = \frac{1}{2}\left(1 + \frac{\mu_R - Q_R}{\mu_R + Q_R}\right) \tag{10}$$

where volumetric flow rate is ϖ and Q is the volume. The mass flow rate can be represented by concentration and volumetric flow rate [38].

$$\dot{m} = \sum_{i=1}^{n} \dot{m}_i = \sum_{i=1}^{n} C_i Q_i \tag{11}$$

$$\frac{\dot{m}_i}{\dot{m}} = \frac{C_i}{C_s}\frac{Q_i}{Q_s} \tag{12}$$

$$\frac{\dot{m}_{thin}}{\dot{m}} = \frac{C_{thin}}{C_{thick}}\frac{Q_{thin}}{Q_{thick}} \tag{13}$$

The concentration, C, and the volumetric flow rate, Q, are compared to the ratio of the mass rates, $\dot{m}$.

Weigl et al. [39] reviews the possibility of a non-instrumented microdevice. The fluid movement would rely on gravity or surface tension rather than an external pump with a power supply. The argument is made for low-cost, rural healthcare though these points are relevant to space exploration missions. Stability until use is an advantage though the simplicity may make them less sensitive at detecting specific molecules (or antibodies or antigens). Multiple streams of fluid can pass through at once where the smallest particles diffuse the furthest across the channel in the same amount of time.

One group of researchers investigated the interaction between three fluid streams. The middle stream is sandwiched between streams of the same fluid so the total volumetric flow rate for the two fluids is constant and equal to the two-stream model, but the surface area between the fluids is doubled, thus increasing the length/area where diffusion can take place [40]. Due to the buffering required by the liquid to prevent back-diffusion of the tagged amino acids, this sandwiching of laminar flow layers may not be feasible for the development of the ABN. From a separation for collection standpoint, fluid layering would complicate the geometry, and more than two outlet ports would be needed.

Culbertson et al. [41] present measurements of diffusion coefficients taken with a microfluidic device. The results show an 11% increase from data in literature when measurements are taken under dynamic versus static conditions.

$$\sigma^2 = 2Dt \tag{14}$$

This Einstein-Smoluchowski equation is commonly used for calculating diffusion coefficients, D, with t as the run time and σ^2 as the spatial peak variance. The experimental work to verify their theory uses bovine serum albumin (BSA), which is the protein most abundant in whole blood.

The Hagen-Poiseuille equation as stated by [9] shows that when the pipe diameter shrinks, the pressure must increase to keep the same flow rate.

$$\Delta P = \frac{12\mu LQ}{\pi d^4} \tag{15}$$

The pressure drop, ΔP, is calculated with a fluid of viscosity, μ, and flow rate, Q, in a channel with a length, L, and diameter, d. The same researchers solve for a critical velocity where diffusion dominates over convective mixing [9].

$$V_C = \pi^2 \left(\frac{L}{d}\right)\left(\frac{D}{d}\right) \tag{16}$$

The velocity is calculated from the length of droplets, L, the diffusivity, D, and the microchannel depth, d.

Choban et al. [42] used a T-sensor (though with inlets positioned in the shape of a "Y"). This shape was thought to shorten the entrance length of the stable velocity profile so the entrance length should be a design consideration if there is not a structural separation at the inlet of the channel.

Mixing:

Ignoring the limits of the dimensions of the channel geometry and any structural flow obstructions in accordance with the flow rates, mixing may occur between the fluids

rather than simply allow for diffusion of molecules between the streams. The work of Adeosun and Lawal [13], Mengeaud et al. [14] and McKay [43] use these mixing theories purposely to induce the fluid streams to combine. Not only do they prove this mixing mathematically, but they also use CFD modeling accompanied by experimental results to show that mixing can and will happen under the correct conditions.

Nonino et al. [44] change the geometry of the flow channels to cause mixing of fluids. For this research, mixing is not desired though changes to the diffusion time are. Jayanti et al. [45] simulate curved ducts by "applying" a centrifugal force to flow in a straight duct. Errors only occurred when the radius of the bend neared the radius of the duct. With electrophoresis, Culbertson et al. [46] used a spiral channel to perform separations. These are unlike this dissertation as separation occurs with natural diffusion instead of an electric field.

Solehati et al. [47] model mixing within the diffusion channel of a T-sensor with Gambit and AutoCAD software. The amplitude of the curving geometry of the diffusion channel changes the flow conditions as well when a T-sensor with a straight and a curvy diffusion channel is modeled to show the possible mixing effects due to geometry constraints. The channel geometry is extremely similar in magnitude and shape to the model presented in Chapter 3 with a width and height of 500 microns. Water was the fluid used for this model.

Some considerations of the fluid mechanics within the microdevice design include rounded bends as opposed to zigzag patterns [35]. Mixing only occurs via diffusion, and as the Peclet number increases, so does the channel length to carry out the diffusion.

Tabeling [48] also refers to mixing as a capability of microdevices. The geometry plays the largest role in causing mixing when laminar flow in microdevices generally is the main reason for using such microdevice technologies. With the Peclet number, the larger the value, the more likely mixing will take place. This value could serve as a check for certifying the fluid streams do not mix and particles in the fluid do not disrupt the flow. Depending on the controls and inlet geometry, it would be possible to form bubbles in the channel.

Effects of particles:

Purcell [11] proposed that small particles act because of the forces on them at the time and not the forces that once acted upon them. This is simply because little inertia exists at low Reynolds numbers for them to continue moving. What this does not take into account is any buoyancy or gravitational effects on the particles for settling purposes.

The motion of spherical particles in film flow is investigated by Pozrikidis [49]. The results, while verified, represent flow down an inclined plane with assistance from gravity. The results of film flow are not directly comparable to flow within a duct.

Brody et al. [10] point out that proteins tend to adsorb to channel walls causing biofouling and eventual clogging. Though amino acid chains may be present in the samples the ABN processes, adsorption to the walls may aid in particulate clumping, which is not beneficial for this system. Because there is a larger surface area to volume ratio in microdevices, the adsorption is more problematic than in larger devices. The adsorption ratio, A_p, was predicted as shown below [10].

$$A_p = \frac{1}{r^2 Cw} \tag{17}$$

The protein radius, *r*, concentration within the flow, *C*, and ratio of volume to surface area per length of channel, *w*, are all needed for this calculation. Brody et al. [10] also show that with low Reynolds numbers, the effects of the wall on particles is much more pronounced than if the particle was in a highly turbulent flow and exhibiting a boundary layer at its surface. The H-filter works similar to field flow fractionation. Their H-filters were 1 mm long, 50 microns wide and 30 microns deep where a pressure drop of 2 cm of water is present between inlet and outlet columns at a flow rate of 100 microliters per minute.

Brody and Yager [50] begin to investigate the size of particles versus their time of diffusion. They also calculated the distances proteins travel across a channel in one second. This model is verified through experimental work where diffusion through a microchannel is observed. The channel is machined from a silicon wafer, and the diffusion prediction is modeled from a Gaussian distribution. The pressure difference between inlet and outlet ports was 3 cm of water to target the flow rate to 100 microns per second for a diffusion rate of 1 second across a 10-micron wide channel; this is compared to 10 days to diffuse across a 1-cm pipe at the same temperature.

Soil movement:

Most of the literature containing information regarding movement of solids either resides in medical or metallurgy journals. Two major issues regarding solids in fluid flow are clumping and settling. Clumping mainly occurs when particles are not spherical, such as red blood cells, or other biological reactions are taking place, such as clotting of platelets in whole blood. Settling is an issue when the particles are denser than the suspending medium or solvent.

One major concern with whole blood is its preference to clump while in channel. This clumping is also a potential concern for moving soil particles through the microchannels, especially from the SCWE chamber to the H-filter where particles may have fallen out of suspension as the ice plugs are allowed to melt before the fluid is pushed through the H-filter. A major difference between medical devices and the ABN task is the fact that blood is a non-Newtonian fluid so any blood data from the literature will not be a reliable comparison to the modeling results from this water and acetone system.

To overcome the settling issue, which is much more relevant to the ABN, it is possible to settle out the large particles prior to the flow in the diffusion channel and only flow particles that are easily suspended due to their shape or density. Another possibility is having a fast enough flow rate that the particles do not have a chance to settle during their resident time within the detection channel.

Priest et al. [51] built a detector for mining companies to use in order to forecast the amount of a targeted mineral present in a rock outcrop. Their microfluidic device had a physical barrier at the bottom of the channel to help keep the streams separated. Settling in the device was also an issue so large particles were settled out of solution before liquid was passed through the microfluidic channels. Priest et al. [52] also showed extractions from between co-flowing streams with 180-micron aggregates present with a continuous flow condition that is assisted by a small ridge at the fluid interface within the channel.

Chen and Jiang [53] and Cal-Prieto et al. [54] use a soil slurry to analyze heavy metals within a soil sample. Ultrasonification and dilution were key to suspensions for quantifying heavy metals with a propensity to settle quickly.

Pozrikidis [49] highlights particle motion in viscous flow, though most specifically in film flow. This does not apply to the majority of the flow seen in the microchannels.

Sub-critical Water Extraction (SCWE):

The SCWE process exists as a way to make water act like an organic solvent instead of using acid hydrolysis. For planetary exploration, utilizing an alternative to organic solvents is appealing; the risk of organic solvents includes leaks to the atmosphere (pollution on another planet or moon) or false detection. Water begins to behave like a nonpolar organic solvent at high subcritical temperatures, which allows for chains of amino acids to be broken into smaller molecules without destroying or diminishing the quality of the sample.

Amashukeli et al. [55] designed, fabricated and tested a portable SCWE in the Atacama Desert. They successfully extracted amino acids from soil using water at the optimal subcritical conditions of 200°C and 17.2 MPa. The SCWE process lasted for a period of 10 minutes to maximize the potential of smaller molecules. The equipment was quite large to hold up to this extreme pressure. The pressure and temperature increases were performed in increments to ensure water stayed in its liquid form.

Depending on the conditioning step following this SCWE process, the water may be warm enough to vaporize the acetone as they flow side-by-side in the H-filter. Keeping the fluids at an increased temperature to decrease the dielectric constant and enhance the ability of water to make amino acid molecules available for further processing must be balanced with the possibility of vaporizing the liquid in the channel. Figure 10 shows the change in the dielectric constant of water from 0°C–100°C.

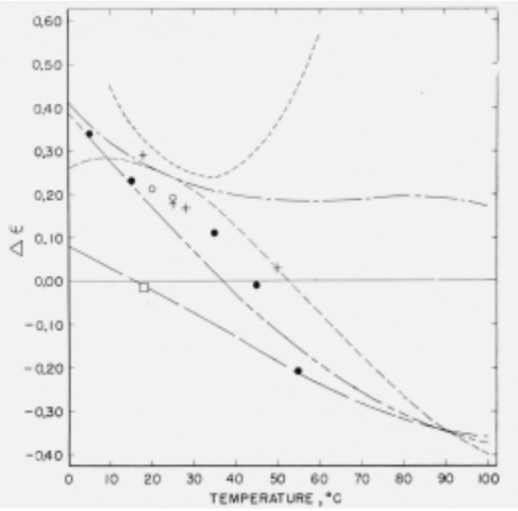

Figure 10. The change in the dielectric constant of water due to rising temperature from various sources [56].

Amashukeli et al. [57] proved the flow rate is also important else sufficient time may not allow extraction to take place.

The SCWE process uses a sealed volume of water with thermal energy added at increments while the pressure builds. If heat is added before the pressure can balance, vaporization may take place.

Effects of heat transfer:

Heating within the channel will affect the thermophysical properties of the fluid and the ability of the molecules to diffuse between the streams. The percentage of this heat effect can be as much at ten percent of the total. While this may not seem like much, because this is such a small scale with fine detection limits, this is a relatively large change. New materials are being used that are compatible with a range of fluids and can moderate desired heat transfer rates.

Heat transfer to microchannels with hydraulic diameters ranging from 30–344 microns is characterized by Xu et al. [58]. The Reynolds numbers are higher than what is

projected for this work, but laminar flow exists and allows heat transfer to occur at relatively large heat fluxes when compared to the geometric lengths of the channels.

Urbanek et al. [59] use angled walled microchannels to investigate temperature effects. Though not explained by theory of Navier-Stokes equation, the Poiseuille number increases with temperature in microchannels of 5–25 micron hydraulic diameters.

Heat transfer between two immiscible fluids in theoretical work by Bostic et al. [60] shows the use of finite element analysis to be a valid method for solving flow problems. The research of Avsec et al. [61] flows gas through microchannels. While the variations of thermophysical properties is presented, the results are not valid for liquids since the densities have a weaker dependence on temperature than gases do. Wibulawas [62] relates heat transfer to laminar flow in non-circular ducts.

Microchannel detection:

The detection component is being developed by an optics member of the ABN task; however, detection considerations are noteworthy for ultimate design of the microchannel network. The limitations on the channel design include enough length in the H-filter where enough diffusion has occurred and the scanning across the channel will be slow enough that the diffusion is no longer changing. Most microdevices have a targeted area of the channel where diffusion measurement takes place optically. With a T-sensor, this positioning of the optical detection equipment is important as the fluids mix upon exit from the channel, and a second chance at analysis does not exist.

Detection within the channel is not the only solution for analysis. If the exit streams are parsed and collected, there would be the opportunity to analyze these collections off-

chip. Regardless, the detection is a one-and-done operation; if the diffusion does not work as predicted, the detection may not occur in the right way, thus affecting any analysis that may take place either in the channel or in a collection container after the channel.

Kamholz, Schilling and Yager [63] present research with optical measurements of diffusion within a microchannel. These measurements do not focus on the splitting off for output ports; instead, all exiting fluid is dumped into one collection reservoir. Their setup allowed for a rapid measurement of diffusion coefficients. Experimental results included measurements at five millimeters down the diffusion channel prior to the fluids exiting with a fluorescence detection system. Their research group points out the difference of fully developed versus developing velocities by modeling the flow.

Optical measurements are a common way to analyze flow characteristics without interrupting the flow, and without needing sensitive probes. Fluorescence microscopy has been used since the mid-1990s for visualizing flows [35].

The purpose of not allowing mixing is to be able to concentrate the fluorescing agent without it tagging to the water stream. This can be achieved by providing a buffer solution with a specific pH level. Holl et al. [6] optimized the extraction device by investigating changes to the flow rates and depth of the channel. This study found the optimal setup to be a 50-micron deep channel with a length of 40 mm, which unfortunately will not satisfy the needs of the ABN.

Uniqueness of application for amino acid detection:

Fluorescamine was first introduced by Udenfriend et al. [64] in the early 1970s as a reagent for assay of amino acids. It is determined through their work that fluorescamine has

a reaction time of one-tenth to one-half of a second with primary amines in a solution with a pH of nine. The reaction with water molecules occurs between five and ten seconds to produce a non-fluorescent product. The products fluoresce for several hours. The strength of the fluorescence is dependent on pH. Not many articles discuss how solutions should be buffered for prevention of back diffusion, nor do they account for material substrate limitations.

Space applications ideally use a small footprint and conservative mass margins. Reliability is key to any design with reusability as an added bonus. Making this detection system from borofloat with a way to clean between uses or avoid cross-contamination is vital to the success of the detection.

Skelley and Mathies [65] used fluorescamine to label amino acids during capillary electrophoresis. Their work was analyzed post-SCWE and not through a microdevice with the same requirements as the ABN has. Chiesl et al. [66] increased detection of amino acids by using Pacific Blue in place of fluorescamine. Jandik et al. [67] purified amino acid samples from carbohydrates for detection procedures.

Beebe, Mensing and Walker [68] review applications of microfluidics for biology uses. The Reynolds number describes the flow regime, so with such small volumes moving through small channels, laminar flow is crucial for flow that allows only diffusion. The fluidic resistance is calculated through geometric measurements and the viscosity of the fluid.

$$S = \frac{12\mu L}{xw^3} \tag{18}$$

The length, L, width, x, and height, w, of the channel along with the viscosity, μ, of the fluid provide the resistance value, S.

Hatch et al. [25] outline a variety of techniques used to analyze molecular binding interactions. For their purposes, a rapid and high-throughput analysis is essential with an existing diffusion potential created by placing the wanted molecules in only one fluid stream. Their device has pressure-driven flow with a range of analytes for testing purposes. They illustrate the difference between premixing the proteins with the analyte. Separation creates very large particles near the interface. Holl et al. [6] walk through the design of a microdevice that extracts albumin (a protein in blood). Their work uses two fluids where detection is the goal for the extracted protein.

Hatch et al. [69] developed a T-sensor capable of measuring molecular concentrations in one minute at nanomolar levels. Though using blood samples for verification, they point out that albumin is known to interfere with the indicator molecules.

Blood clumps on its own and has a tendency to adhere to the channel surfaces [10]. Some devices use filters or centrifugal force to separate particles from soluble components [33]. It is also noted that the size of the particles directly relates to the point at which they cross into the second stream along the length of the channel making it possible to sort particles by size based on the distance down the length of the microchannel. This will be helpful for when the amino acids are tagged by the fluorescamine, which will create a larger molecule to separate into its own flow.

Mora's group [70] used capillary electrophoresis to detect organics. Amino acids are targeted for their composition and structure. Movement on the chip occurs through peristalsis with actuated valves. A large footprint is needed for the external instruments providing assistance with microchip operations. Skelley et al. [71] extracted amino acids from bacterium. Their system runs a rinsing solution through after each analysis so must

take extra fluid. Experiments show pH values matter when it comes to intensity of the fluorescence, and the total time was 12 minutes with 10 minutes for labeling and two minutes for separation.

Kate et al. [72] studied the photostability of amino acids to predict length of exposure to UV radiation on Mars. If embedded, the amino acids could last several thousands of years yet when exposed at the surface, the amino acids most likely could not last one day. This is important to note, as samples of soil cannot be simply scooped from the surface of Mars.

Experimental data:

The data shown in Table 1 are results from experiments with configurations similar to the ABN. These experiments range from two fluids to three fluids. The geometry is only different in the entrance portion of the device; the fluids still flow side-by-side in the diffusion channel. Some include the use of membranes between the fluids or films on the channel walls to absorb specific molecules, or cause or limit a reaction. Data were used for fluorescamine and fluorescein with BSA as well as non-fluorescing reactions. Some of the literature include data from blood analysis. The channel dimensions and flow rates are included for replication in the validation section in Chapter 5. Not all sources listed in Table 1 share the diffusion coefficient used in their modeling. When this occurred, the diffusion coefficient was looked up in other references. Some of the sources shown in Table 1 are not used for validation; these sources do not provide a reaction with non-Newtonian behavior, which is different than flowing amino acids in water. Other sources also note fouling on the channel walls, and as the device should be reusable, fouling hinders this requirement.

Table 1. Device experimental results from literature.

Materials	Dimensions	Flow Rate	Results	Reference
Albumin, water	<100micron(z), <100micron(x)	0.1 and 0.25 μL/s	Graphical output	6 (1996)
2.6- and 12-micron diameter spheres	50micron(z), 200micron(x)	100 μm/s	Fluorescent image	7 (1996)
HCl, NaCl, NaOH, CH_3COONa	69micron(z), 160mm(y), 404&266mm(x)	$3.85x10^{-9}$ and $3.85x10^{-10}$ m^3/s	Plots from model	8 (2012)
Cytochrome, sodium benzoate	Various ratios	Various ratios	Graphical output	18 (1992)
Albumin, creatinine	330micron(z), 4.45micron(x), 22.2mm(y)	83.3 nL/s	0.81 s	19 (2011)
Creatinine and albumin	n/a	n/a	Graphical output	20 (2005)
BSA + antibody (1–1000 nM concentrations)	0.3mm(x), 3mm(y), 0.1mm(z)	53 nL/s	Pictures and plots	23 (2007)
Fluorescein-biotin + BSA	1560micron(x), 92micron(z)	20.8 nL/s	Graphical output	25 (2004)
Ink and water	100micron(x), 50micron(z), 10–20mm(y)	n/a	Picture and graphical output	26 (2007)
Hexane and oil	150micron diameter	0.1 mm^3/s	Picture and 4.8 s	29 (2006)
HAS, albumin blue	550micron(x), 25micron(z)	83.3 nL/s	Optical output	34 (1999)
Tanshinone IIA, dichloromethane	600micron(x), 30micron(z)	0.2 mL/min	Picture and plots	40 (2010)
Fluorescein-biotin	75micron(x), 10micron(z)	41.7 nL/s – 1 μL/s	Optical measurement	63 (2001)
Water, rhodamine B	50micron(z), 100–200micron(x), 4mm(y)	1.2–20 μL/min	Pictures and plots	73 (2009)

Brust et al. [74] focus on the plasma portion of blood. Only surface effects exhibit non-Newtonian behavior in plasma and bovine serum albumin (BSA). These effects are also present with changes in pressure, which means the viscoelastic behavior of plasma is important in assuming Newtonian behavior.

Mu et al. [40] extract herbal ingredients from plant matter at an improvement rate of over 90% by switching from solvent extraction to microfluidic device extraction. Van Leeuwen et al. [73] use an H-filter to transfer glucose between two streams of water. The LFDI needs to be stable, predictable and split correctly at the outlet. Flow simulations were performed in COMSOL for a rounded diffusion channel and compared to visual data from the flow.

Fluorescing agent:

Corresponding states work includes the comparison of two or more fluids from the same family (similar molecular structure) and their thermophysical or transport properties. This allows for the comparison of two fluids where the properties of one are not known very well. The chemical structure of fluorescamine ($C_{17}H_{10}O_4$) is shown in Figure 11.

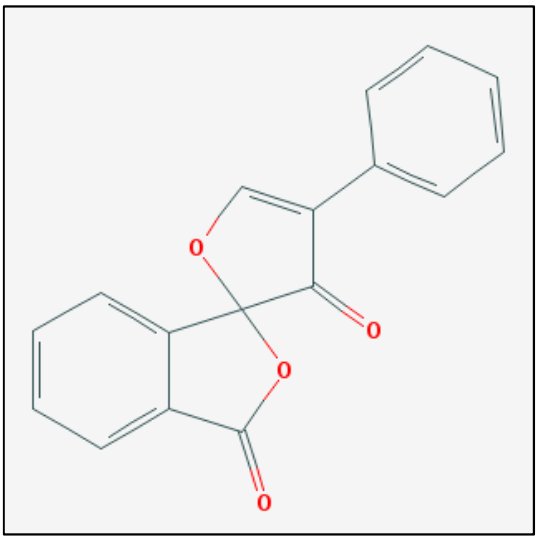

Figure 11. Fluorescamine molecular structure, $C_{17}H_{10}O_4$ [75]

This fluid is an identified fluorophore with a known range of fluorescence activity based on wavelength yet thermal effects and most properties are unknown. Figure 12 shows its reaction with a primary amine.

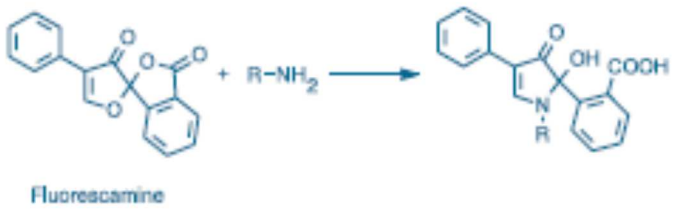

Figure 12. Fluorogenic amine-derivatization reaction of fluorescamine [76].

Culbertson et al. [41] show that diffusion coefficients are measured using devices such as the H-filter or T-sensor. Their experiments use fluorescing agents showed a slight interaction between the fluids and the channel wall with static measurements.

Hausler et al. [8] optimized the design of an H-filter by the resulting Fourier number. Each aspect ratio of the channel dimensions was compared to the flow of a solution whose diffusion coefficient was measured. The results agreed closely to literature, and diffusion times ranged between 3–14 seconds.

Fabrication:

Kenis et al. [77] used chemical etches flowing through the microchannels to show that 5-micron features are possible to manufacture with the correct combination of flow rates and chemicals.

Stockton [78] outlines the fabrication process used most commonly by device engineers at JPL. This is the procedure used for manufacturing the features for the ABN.

While chemical etching produces clean walls, defects may be present during bonding of the two discs, and mostly limited to the corner of the channel.

Work in this dissertation:

The work outlined in subsequent chapters builds on the existing work of H-filter theory. It incorporates a chemical reaction between particles in the two fluid streams and takes into account overall temperature of the system. (The range of temperatures including high, low and average are investigated separately for the outcome of the calculated diffusion coefficient.) The temperature affects transport and thermal properties. Wall effects are ignored since eddy currents from wall temperature fluctuations could theoretically form.

Chapter 3: Modeling Fluid Flow

The modeling of the diffusion effects of the AstroBioNibbler is focused on the diffusion channel portion of the H-filter. The model assumes that diffusion starts to occur once the bulk fluid begins to travel down this diffusion channel without residual effects from the inlet conditions. Inlet effects are important though with laminar flow, and with a small geometric addition to help the flow turn 90° against a partition rather than the opposing fluid, any undesired effects (such as mixing of the fluids) can be minimized or eliminated.

Modeling considerations:

Time and spatial values can be used to designate the flow conditions and corresponding concentrations with MATLAB modeling. These incremental values of time and space are small in comparison to the size of the channel as well as the flow rate and molecular length in order to minimize error propagation.

Constants:

Water and acetone are the fluids moving through the H-filter. The temperature range expected by the device is from room temperature and atmospheric pressure to approximately 500 K at a pressure of 240 kPa to keep the fluids in liquid phase. Figures 13 and 14 show the vapor pressures for acetone and water.

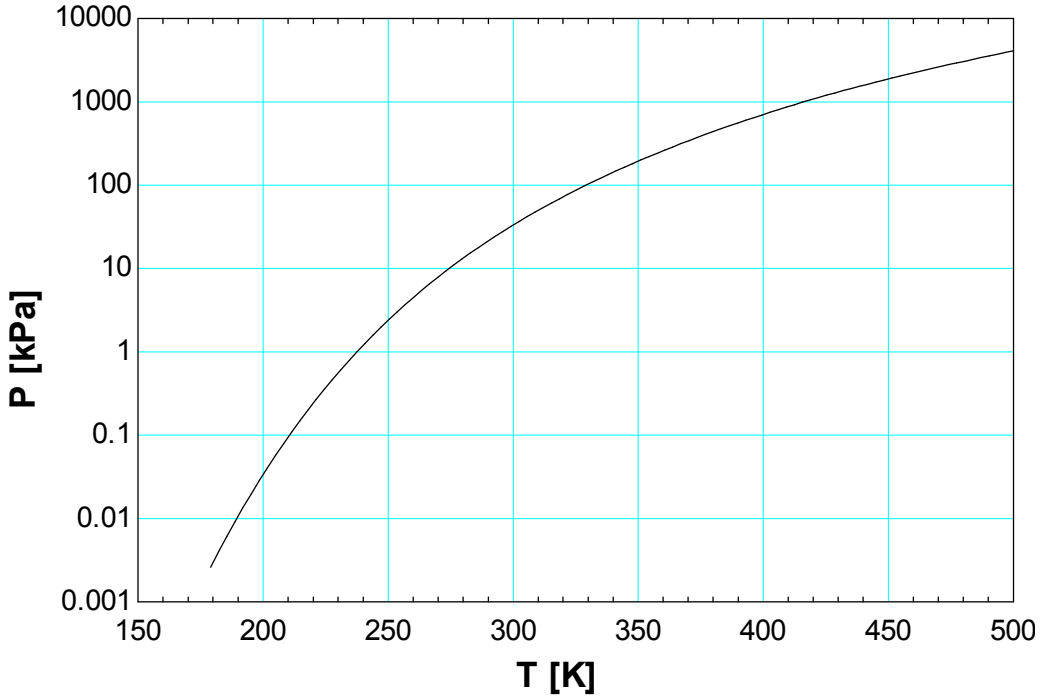

Figure 13. Vapor pressure data for acetone as plotted in EES using the equation of state developed by Lemmon and Span [79].

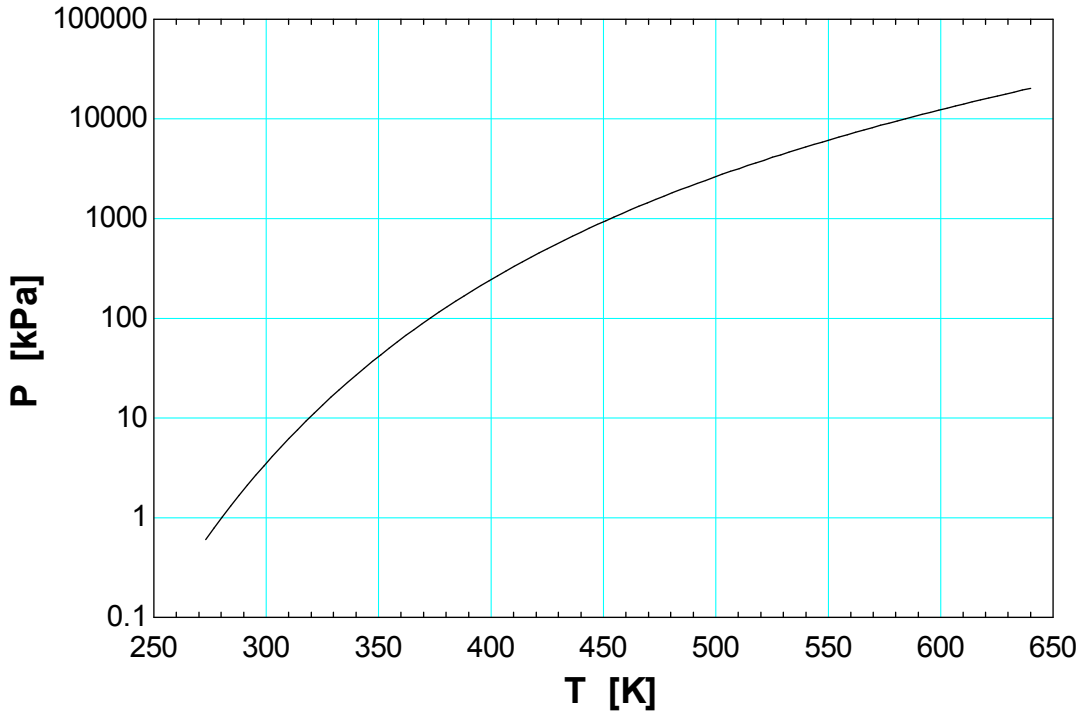

Figure 14. Vapor pressure data for water as plotted in EES using the equation of state for water developed by IAPWS [3].

These high temperature/pressure limits occur on the SCWE chip and not near the diffusion channel although it could be possible to add the capability of using excess heat to help the diffusion occur at a more rapid pace. It is noted that the effects of temperature fluctuations on reaction kinetics are not discussed in this work.

Inlet conditions:

The inlet fluids of acetone and water enter the H-filter as opposing streams. The pressure of each stream must be balanced so that one fluid does not dominate the diffusion channel. Both fluids flow at velocities proportional to the viscosities of the fluids in order to have the same pressure drop along the length of the diffusion channel. Having similar pressure drops causes the LFDI to be at or near the centerline of the channel and will help the optical detection avoid the walls of the channel, the consequences of which are discussed in Chapter 5. As shown by Equations 8–13, the viscosity of each fluid will determine the relative velocity of the fluid streams. No geometric constraints are needed for the inlet though having a physical barrier to help turn the opposing inlet streams 90° to run parallel to each other would ensure no mixing happens or that particles do not impinge on the other fluid through momentum rather than diffusion if particles are carried by either fluid. Rounding the corners would eliminate eddy formation at the inlet. The velocity at the LFDI must be the same for each fluid.

Diffusion channel:

Once the fluid turns 90° from the inlet to begin flowing in the diffusion channel, the velocity profile stabilizes. This entrance length is calculated by Equation 19

$$L_E = 0.05ReD_h \tag{19}$$

where the Reynolds number, *Re*, and an equivalent hydraulic diameter, D_h, are used to verify the point in the channel at which the velocity profile will not change. The Reynolds number is used to verify the flow conditions and is calculated from the velocity, cross-sectional length and viscosity of the fluid as given by Equation 7.

Table 2 lists the flow conditions exhibited by each fluid at different flow rates.

Table 2. Calculated Reynolds numbers for varying flowrates.

Water (Pr = 7.18)			Acetone (Pr = 4.22)		
Flow rate [μL/s]	Reynolds number	Pressure change [Pa]	Flow rate [μL/s]	Reynolds number	Pressure change [Pa]
1	0.05514	1.324	1	0.136	0.4252
2	0.1103	2.649	2	0.272	0.8503
5	0.2757	6.622	5	0.6801	2.126
10	0.5514	13.24	10	1.36	4.252
25	1.379	33.11	25	3.4	10.63
50	2.757	66.22	50	6.801	21.26
75	4.136	99.34	75	10.2	31.89
100	5.514	132.4	100	13.6	42.52

The values listed above are calculated with a temperature of 293 K and a channel width and depth of 300 microns (flow area is half of total channel). The flow rates are expected to be under 5 μL/s, and for both fluids, the Reynolds number is under 10 at that rate. The entrance length is less than 5 μm at a Reynolds number of 5; this entrance length is less than 0.025% of the channel length.

The pressure drop, as stated by Equation 15, can also be stated equivalently below

$$\Delta P = f_D \left(\frac{L}{D_H}\right) \frac{\rho u^2}{2} \tag{20}$$

where pressure drop is function of friction factor, f_D, (for laminar flow where $f_D = \frac{64}{Re}$) and the ratio of the length over the diameter. For this case, values shown in Table 2 do not change much over a range of flow rates when compared to the atmospheric pressure of 101,325 Pa. If on Mars, the pressure is even lower at 600 Pa, and the pressure drop would be approximately 1% over the length of the diffusion channel between the inlet and outlet.

In configuring Equations 4, 5 and 6 to solve directly for the shear stress, and solving the velocity profile across the channel for two adjacent fluids with differing viscosities, the results are shown in Figures 15 and 16. The velocities are the same value at the interface. The maximum velocity location is also where the shear stress is zero, as expected.

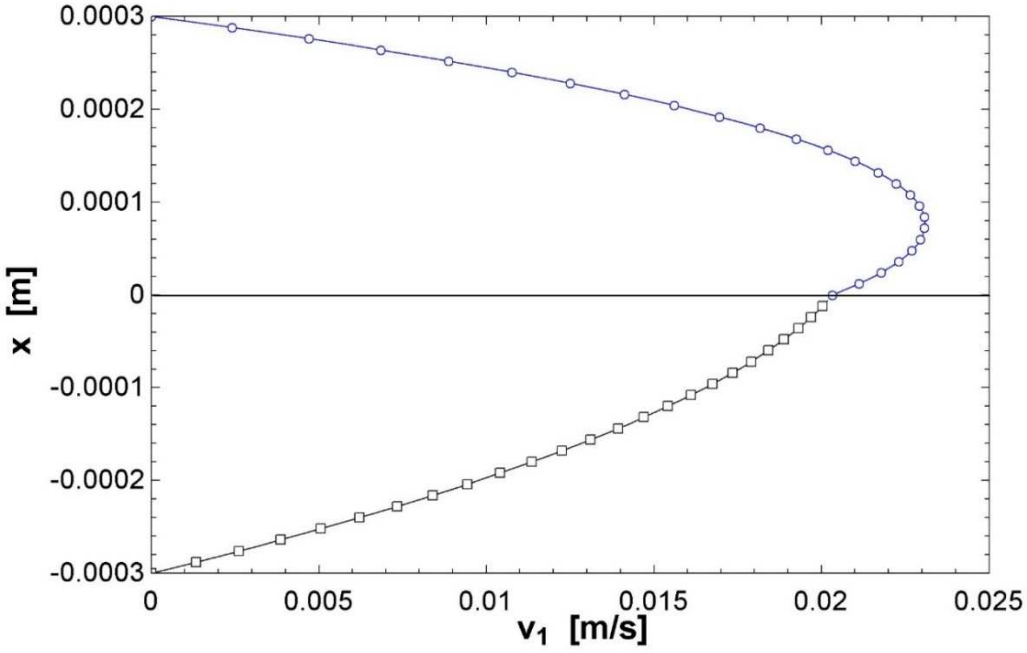

Figure 15. Velocity profile in flow. Top fluid is acetone. Bottom fluid is water. Results of Equation 4 [15].

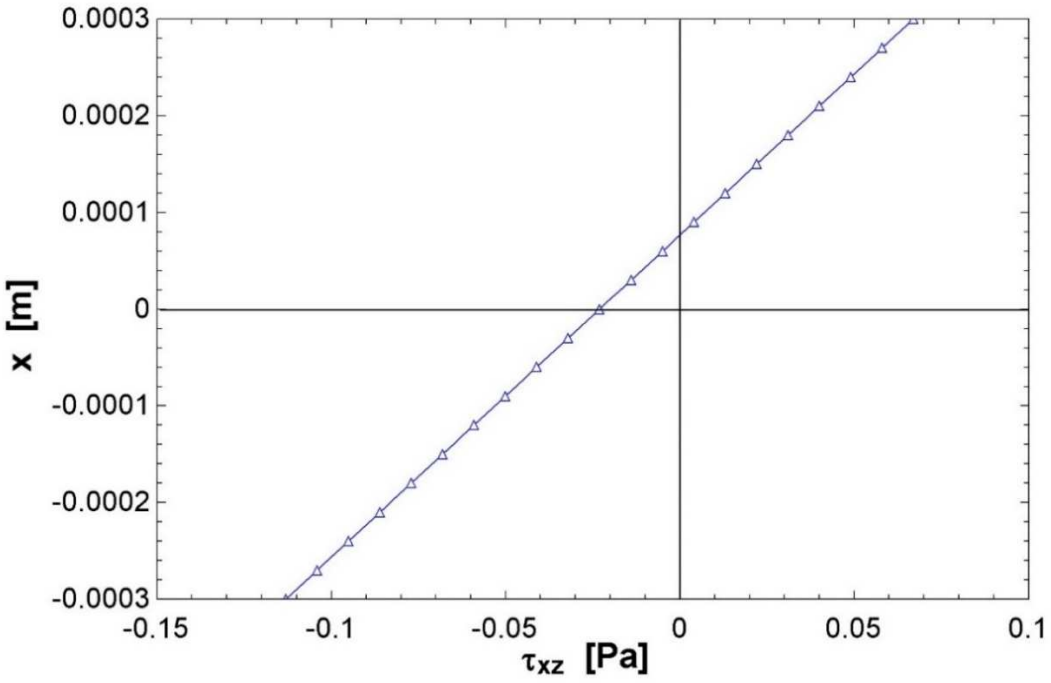

Figure 16. Shear stress of same flow conditions with water on bottom and acetone on top of channel. Results of Equations 5 and 6 [15].

These graphical representations show what is occurring as a bulk fluid. Discussion for mass transport is included in Chapter 4.

Outlet conditions:

The end geometry separates the streams largely based on viscosities of the fluid streams. Knowing where the particles within the flow occur crosswise, the correct ratio of exit stream geometries may be calculated for various separation needs. This would allow for concentrating the fluorescing stream to ensure all fluorescamine finds an amino acid with which to react, or it allows dumping all or a part of the exiting fluid to a waste stream.

Chapter 4: Modeling Mass Transfer and Thermal Effects

Partial differential equations were used for the diffusion equations relevant to this model. Fluorescamine and amino acid chains are the molecules carried by the fluids, water and acetone, respectively, and they are the molecules being modeled for concentration profiles. The conservation of chemical species is represented by Equation 21 with three dimensions of concentration rates, where C is the concentration, t is time, D is the coefficient of diffusion.

$$\frac{\partial C}{\partial t} = D\left(\frac{\partial^2 C}{\partial x^2} + \frac{\partial^2 C}{\partial y^2} + \frac{\partial^2 C}{\partial z^2}\right) \tag{21}$$

The directions are represented with x as the direction of diffusion across the channel width, y as the direction of diffusion along the channel length, and z as the direction of diffusion along the channel height. The z-direction is deemed negligent due to low gravity effects. The transient nature of the equation allows a simple model to be built using the correlation that flow rate down the channel can be exchanged for the y-direction component of this concentration as the model solves each time step. The remaining equation is also known as Fick's Law.

$$\frac{\partial C}{\partial t} = D\frac{\partial^2 C}{\partial x^2} \tag{22}$$

The initial condition is a step function where the concentration of the amino acids begins at 1 on the left side (100% concentration) and 0 on the right (0% concentration) within the stream of water.

$$C_{x<\frac{w}{2},t=0} = 0 \tag{23}$$

$$C_{x>\frac{w}{2},t=0} = 1 \tag{24}$$

The concentration is normalized to 1 for the rest of the problem. The reverse initial conditions are true for fluorescamine because it starts in the acetone and is allowed to diffuse to the water side.

The boundary conditions set the derivatives along the sides of the channel at zero where no mass can enter or leave, or a zero flux condition. The boundary condition is Equation 25.

$$\frac{dC}{dx}_{x=0} = \frac{dC}{dx}_{x=w} = 0 \tag{25}$$

This is true for all values of *t* at $x = 0$ and $x = w$. The channel wall is not permeable for the case of the ABN. There is not a boundary at the centerline as most flow problems would have since there is no symmetry between the diffusion of these molecules into a fluid different than the molecule's carrier fluid. Observation of what occurs at the interface between the fluids is a good check; their velocities must match, and no discontinuities should occur.

The spatial and temporal steps (appearing as ∂t and ∂x in the above equation) must be on the same order else oscillations occur and skew the solution. The equations used within Equation 26 uses forward time marching, central differences to calculate the concentration along the channel.

$$C_i^{n+1} = C_i^n + D\left(\frac{\Delta t}{\Delta x^2}\right)(C_{i+1}^n - 2C_i^n + C_{i-1}^n) \tag{26}$$

The indices of *i* and *j* represent the time and position coordinates as the concentration is known and calculated. Each molecule has its own concentration model based on Equation 26. A third concentration results from the formation of an additional molecule from the reaction of an amino acid with a fluorescamine molecule.

Fluorescamine binds with water molecules 100% of the time they come in contact with each other. However, the rate of the reaction is 10–100 times faster between fluorescamine and amino acids than between fluorescamine and water. The assumption was made that as long as fluorescamine is in the same part of the fluid where amino acids can be found, the reaction occurs between the two instead of fluorescamine binding with water.

Diffusion coefficients:

One difficulty searching for fluids and molecules for a fluorescing reaction is the lack of experimental data for molecular properties, mainly the lack of verifiable diffusion coefficients. There is evidence temperature can shift the value of the diffusion coefficient. Fluorescamine is not as well-known as fluorescein, but with a similar molecular makeup and structure, the general characteristics for fluorescamine are verified by comparing it to fluorescein.

The diffusion coefficients are calculated using Equation 7. Both fluorescamine in acetone and amino acids in water are calculated with temperature dependence. This equation is a way to relate unknown diffusion coefficients. Though it is not a true corresponding states work, the possibility of the diffusion coefficient as a function of temperature, viscosity and molecular size is important. The best/worst case scenarios with the amino acids are to use the largest and smallest molecular diameters within the equation for the diffusion coefficient. Amino acid chains range between 1.2–1.7 nm, and their lengths can also increase or decrease depending on how much water is "held" by the molecule.

Fluorescamine has a molecular weight of 278.26 and a diffusion coefficient of 1.77×10^{-6} cm^2/s in acetone and 6.11×10^{-7} cm^2/s in water (at 298 K) as calculated by Equation

7. None of the manufacturers give coefficients let alone over a range of temperatures, and while room temperature may be a common operating parameter for most applications, it is not for this work.

Fluorescein is a closely related fluorophore with a chemical composition of $C_{20}H_{12}O_5$. Using Equation 7, the diffusion coefficient of fluorescein is calculated to be 3.54×10^{-6} cm^2/s. According to manufacturer's data [80] and Hatch et al. [25], the diffusion coefficient is 4.25×10^{-6} cm^2/s, which means the calculated value is a 17% decrease over the measured value. Over the range of freezing to boiling water (at atmospheric pressure), the calculated diffusion coefficient changes from 1.67×10^{-6} cm^2/s–1.40×10^{-5} cm^2/s, or a factor of ten, and both the calculated and the manufacturer-provided values are within this range. This can be due to temperature effects or an overestimation in the molecular size. For instance, a 40% increase in the molecular size (from 0.5 nm–0.7 nm) results in this same 17% decrease in the diffusion coefficient.

The fluid reactions change with temperature due to the influence on the diffusion coefficient. That change is shown in Figures 17 and 18 for water and acetone, respectively. The diffusion coefficients are inversely proportional to the length of the diffused molecule. Though amino acids can be of varying lengths, an average length was used in the diffusion coefficient calculation.

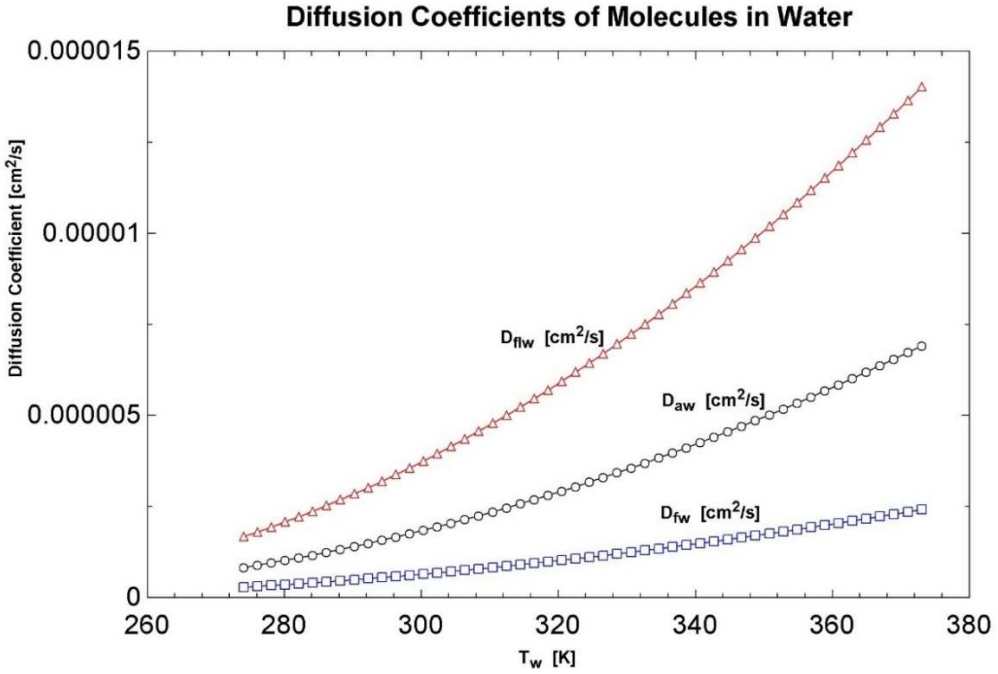

Figure 17. Diffusion coefficients of fluorescamine and amino acids in water.

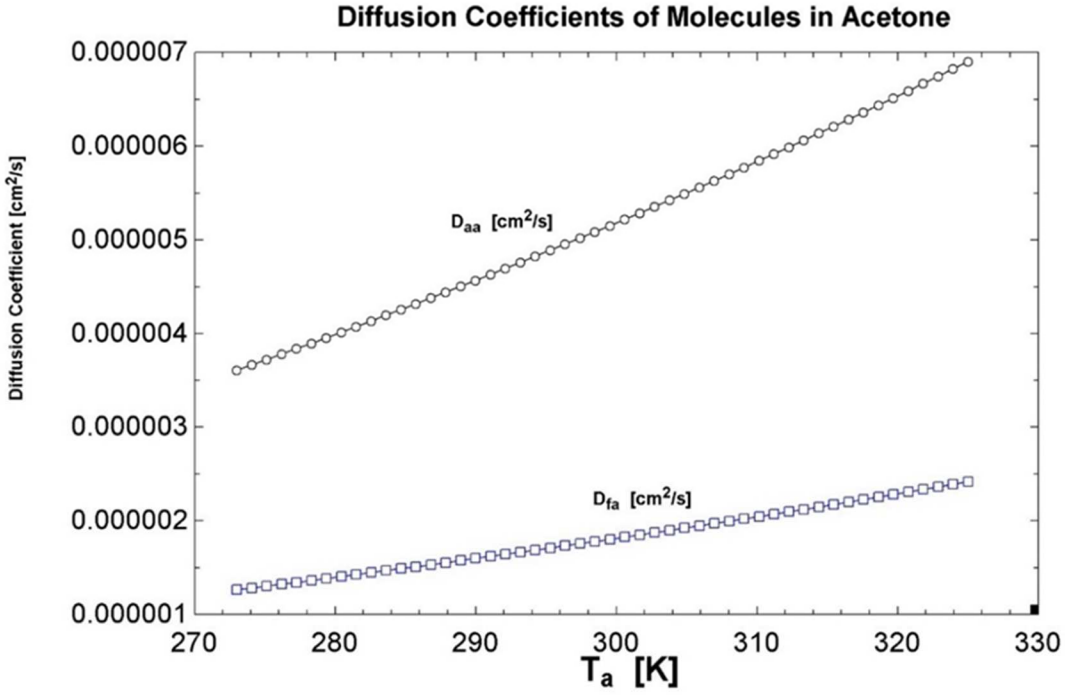

Figure 18. Diffusion coefficients for fluorescamine and amino acids in acetone.

The diffusion coefficients are shown over a range of temperatures at atmospheric pressure. The acetone is the limiting fluid and will vaporize if heated above 327K without additional pressure. The water vaporizes at 373K, which means if heated water comes in contact with the acetone, the acetone can still vaporize. With respect to the diffusion coefficients, the difference due to temperature is very small and does not change the value of the concentration much.

Modeling verification:

The values for the spatial and time steps must be verified for stability of the modeling. The model began with a spatial step of 12 microns. The definition of the corners was not fine enough for molecules on the order of 1.2 nanometers. Reducing the spatial step to one micron maxed out the memory of MATLAB. Using a spatial step of 5 microns allowed a refined resolution along with a reasonable processing time.

The time step was calculated using the von Neumann method for solution stability. The variable *G* is solved between time steps of the concentration value for upper and lower bounds.

$$C_i^{n+1} = GC_i^n \tag{27}$$

After incorporating *G* into the solution of the PDE and substituting *d* as shown in Equation 28, the bounds of the solution become

$$f = D\frac{\Delta t}{\Delta x^2} \tag{28}$$

$$-1 \leq 1 + 2f(\cos\theta - 1) \leq 1 \tag{29}$$

where a 5-micron spatial step for Δx allows for the time step to be equal or less than 0.07 seconds, or 70 milliseconds, when the fluid is water (due to dependence on diffusion coefficient). A selection of one millisecond for the time step is within stability criteria. If compared with the movement the fluid would experience with a particular flow rate, the time step allows enough movement downstream for the concentration to be calculated for a new location during each time step.

Modeling considerations:

The dynamic viscosities of acetone and water at 20°C are 0.0003224 kg/m-s and 0.001002 kg/m-s, respectively. Knowing that the viscosity affects how a specified volume of fluid will move and interact is a critical piece to controlling the design of these microfluidic channels.

At atmospheric pressure, acetone boils at 56°C. If water is entering the channel hotter than the acetone, it is possible the acetone will vaporize. The diffusion can occur at a faster rate if the temperature is higher so for these reasons, it would be necessary to have the pressure at a point where both fluids can maintain their liquid state.

An exact solution is helpful, but for complex modeling purposes, a numerical solution is needed. MATLAB was used for its ability to handle large matrices. The built-in PDE solver was not used at this time. The boundary condition of a zero flux is captured by using an equation that ties the concentration at the edge to the concentration in the stream with a way to mimic a zero-flux condition. Figures 19 and 20 show concentration changes as the fluids travel down the channel. These figures show the way the concentrations begin to level out as the fluid moves down stream.

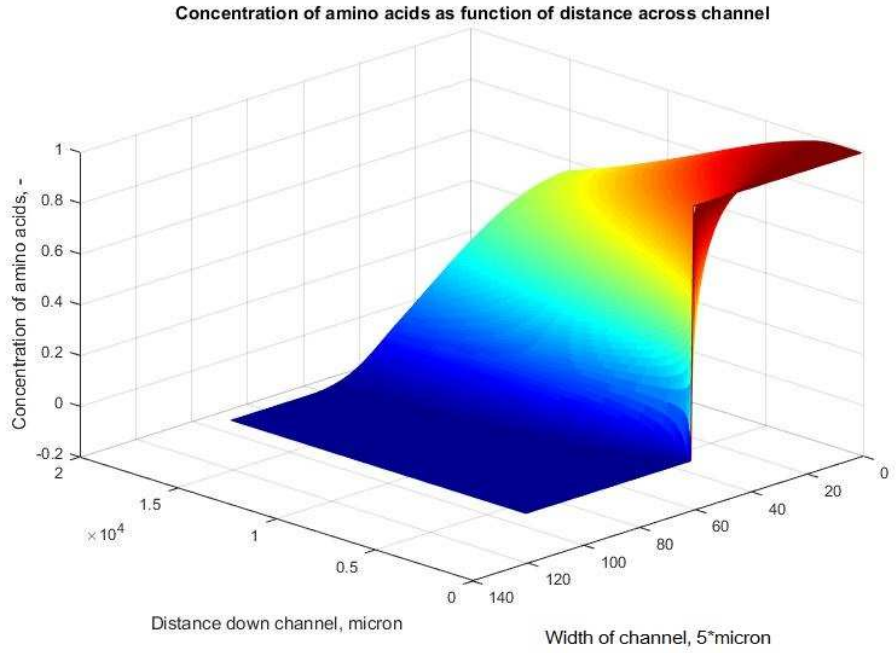

Figure 19. MATLAB graphical output of amino acid diffusion.

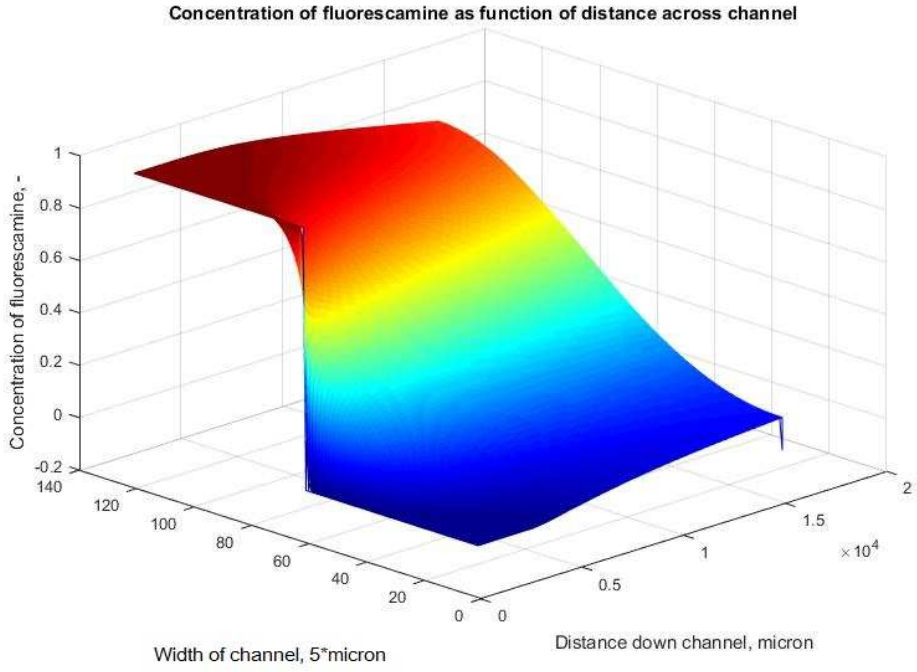

Figure 20. MATLAB graphical output of the fluorescamine diffusion.

Chemistry:

Acetone requires a buffer for the pH level to be balanced to the soil/water slurry. The soil particles average 150 microns as the aim is to complement current sampling drills that produce particles in this approximate size range. Effects of the materials interacting with the fluids are ignored. Wetting and molecular interactions from the channel walls are ignored. No applied electric fields are present. Any heating of the walls occurs as a flux, but for this work, is also ignored. Reactions of fluorescamine molecules with found and available amino acids is considered and shown in Figure 21.

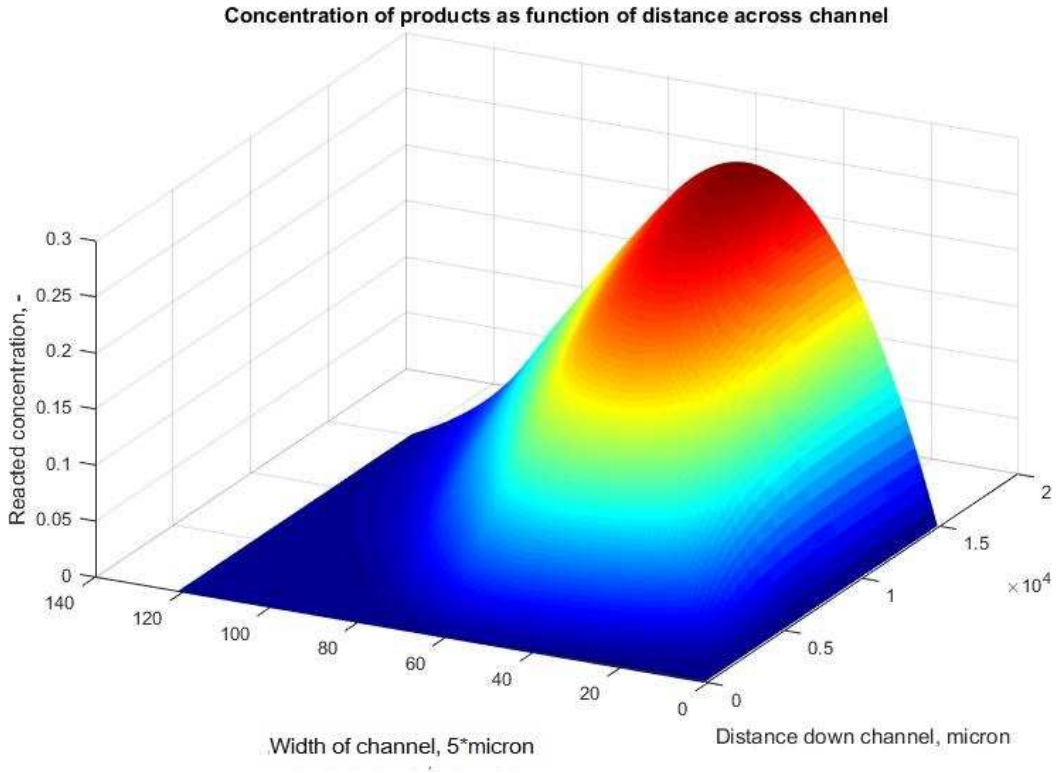

Figure 21. Product from reaction of fluorescamine with amino acid.

The values used in the solution assume a reaction rate of 0.05% when both molecules of fluorescamine and amino acids are present. The model does not eliminate fluorescamine from the channel to mimic its loss to water.

Chapter 5: Results

The model provides an estimation of time and distance the fluorescamine takes to tag amino acids in the diffusion channel. With a flow rate of 1.0 microliter per minute for water and 3.1 microliters per minute for acetone, the fluorescamine reacts with amino acids and fluoresces by the end of the diffusion channel. Since fluorescamine can tag the water molecules, albeit much less likely in the presence of amino acids (at a rate of 1 to 10 in favor of amino acids), the product formed by the amino acid and fluorescamine is measured in the reactant stream. The molecules of this newly formed compound are found on the acetone side by a length of 0.3 mm.

The flow rates vary, and if the flow rates increase to more than 10 microliters per minute, the Reynolds number rises above 1. While this is still laminar flow, the flow at a Reynolds number below 1 is dominated by viscous forces and can take the unevenness of channel walls with a lower rate of disturbance.

The largest contributor to the error in the results is due to the diffusion coefficient. The diffusion coefficient is suggested for amino acids in literature. To calculate the diffusion coefficient, the size of the molecule is needed. Amino acids have a range of lengths though the most commonly occurring amino acids are 1.4–1.7 nanometers long. The length and shape of these amino acids do vary if the amino acid reacts with water molecules. This should not be as great an issue after processing in the SCWE chamber than before processing. The water temperature during SCWE is higher to cause the dielectric coefficient of the water to drop; this helps the water molecules to depolarize and become less attractive to each other and other molecules.

Investigating the effects of temperature on the calculated diffusion coefficients used in the model, for molecules diffusing through water, the value changes 10% with a four-degree temperature increase/decrease. For molecules diffusing through acetone, the diffusion coefficient changes by 10% with an increase/decrease of 8.5 degrees. The temperature change affecting the diffusion coefficient has less of an effect than the size of the molecule.

Literature validation:

Inputs to each of the referenced models were put into this model for comparison of their results to the results of this model. These comparisons of output (a concentration profile at a specific location in the diffusion channel, designated by the reference) are included in Table 3. Not all references in Table 1 included enough information for a proper comparison and are not listed in Table 3.

Table 3. Results from reference parameters run in model.

Best Fit	Average Fit	Reference
20.5%	21.6%	[19] Albumin
0.606%	1.02%	[19] Adjusted
0.962%	4.03%	[25] Fluorescein
1.79%	3.15%	[25] Fluorescein-biotin
0%	6.34%	[34] Low flow
0%	0.27%	[34] High flow
1.98%	16.7%	[63] Low molar
1.98%	7.96%	[63] High molar
0%	1.36%	[73] Rhodamine B

The results in Table 3 are the percentage difference between the modeled results in comparison to results presented by their respective research team. The “best fit” is how close the profiles matched each other at any concentration level. The “average fit” is how close

the entire profiles matched each other at all locations of the channel width. The dimensions of the channel, flow rate, fluids and molecules used in order to find appropriate diffusion coefficients (if not provided by the reference) were used in the model. Slight adjustments were made in the comparison of the model to [19] since the results given by [19] included a physical barrier in the exit of the channel that was not accounted for in the model here.

Each reference is shown below as a comparison of the concentration profile plotted against the results of the model.

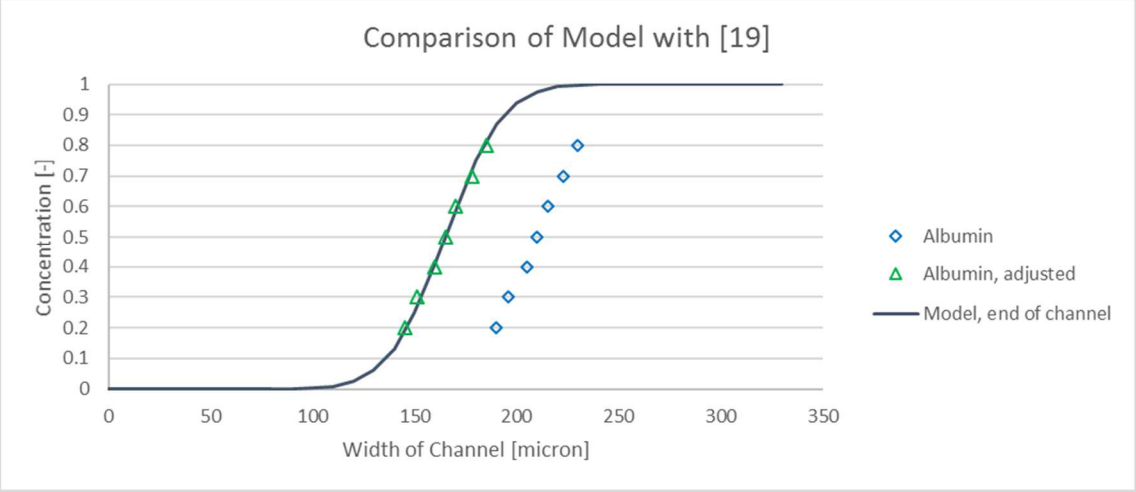

Figure 22. Comparison to Schattka et al. [19] with albumin diffusion.

The profiles in Figure 22 show the difference between the model created here versus the results provided by Schattka et al. [19]. Their model is adjusted for a physical barrier put in place to help separate the exit streams. With this adjustment in place, the error is 2%. Without, the associated error is greater than 20%.

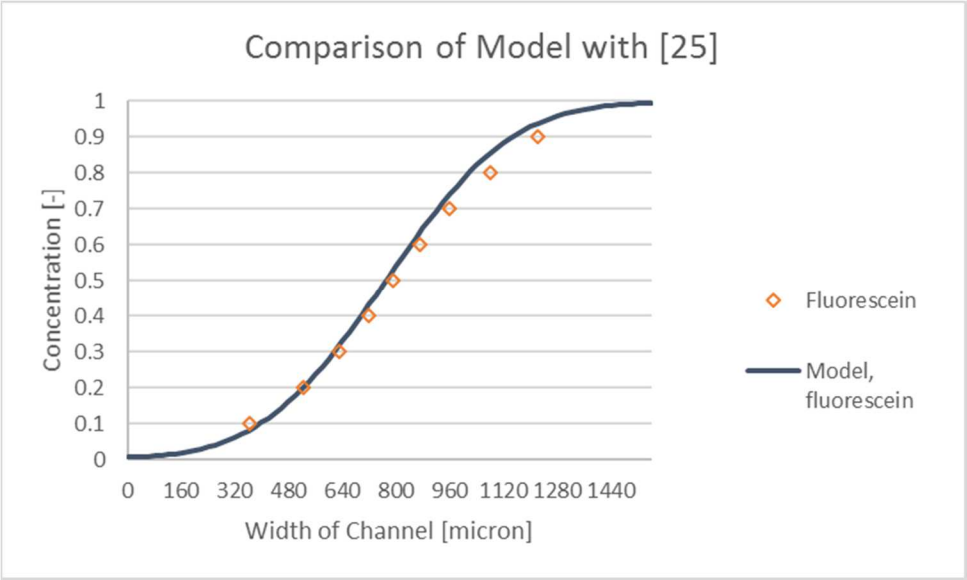

Figure 23. Model comparison to Hatch et al. [25] for fluorescein.

Figure 23 shows a comparison between the model and results presented by Hatch et al. [25]. Fluorescein is of importance in validating the model. With the absence of fluorescamine in the literature and from experimental results, fluorescein is a similar-sized molecule that also gives off fluorescence when it tags to protein chains (or amino acids). The comparison is within 4% until 960 microns (and greater) across the channel width.

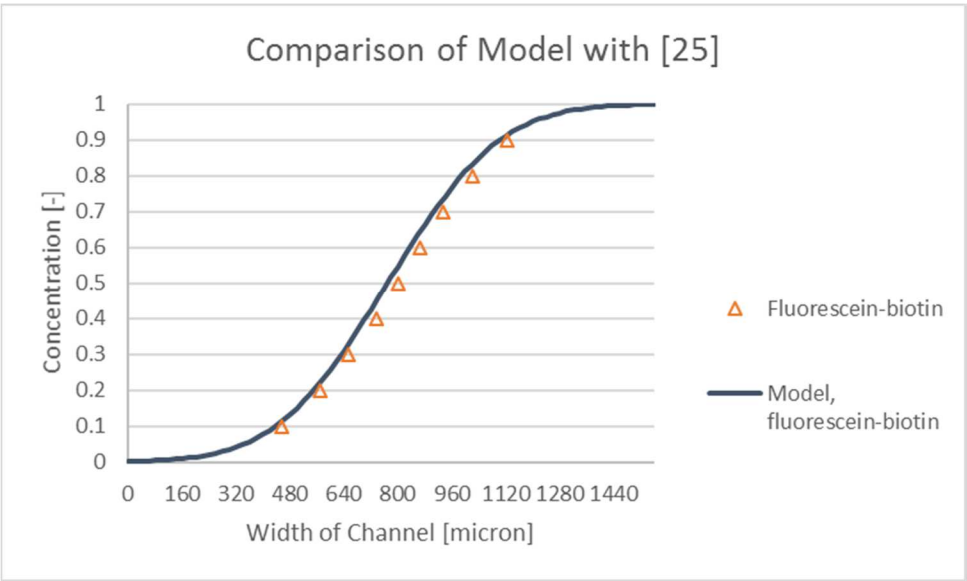

Figure 24. Model comparison to Hatch et al. [25] for fluorescein-biotin.

The fluorescein-biotin results are less deviating from the model and the results of Hatch et al. [25]. The greatest error between the model and the results are 5% or less with most at 2.5% difference.

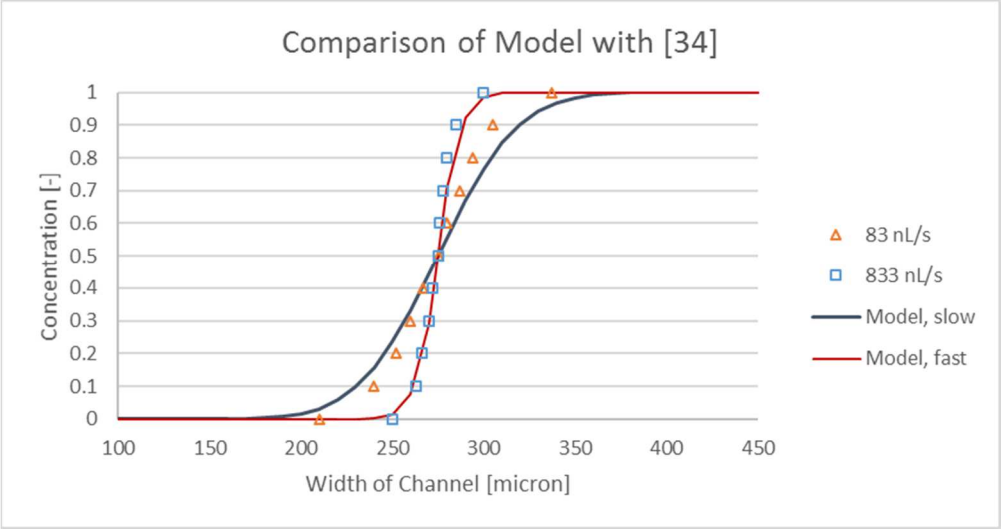

Figure 25. Comparison of model to Kamholz et al. [34] with two flow rates.

Figure 25 shows two flow rates from Kamholz et al. [34] where the faster flow rate is ten times the slower flow rate. The model was set to the slower flow rate, and the error between the two is less than 5% except for where 0% and 100% concentration levels occur. The faster flow rate has much better matching to the model.

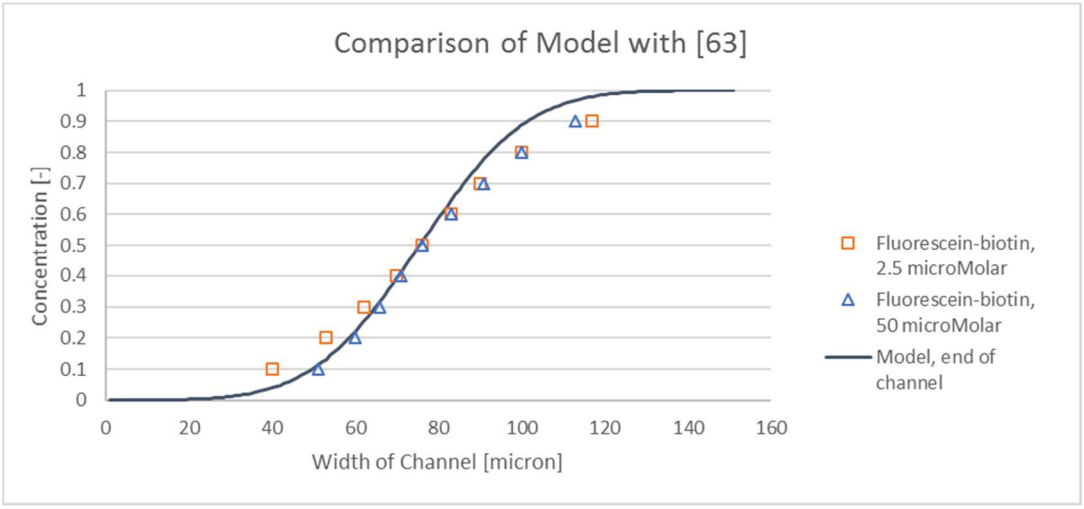

Figure 26. Fluorescein-biotin profiles presented by Hatch et al. [63] in comparison to modeling.

The comparison with visualization in Figure 26 shows a similar calculation for the concentration for the rising side of the channel (the side that starts with zero concentration) at the exit of the channel. The model deviates more for the fluorescein-biotin with a lower molar concentration than for the fluorescein-biotin with a higher molar concentration. The lower molar concentration has an error of more than 30%. The error for the higher molar concentration is 12% or less. The model has no way of taking molar concentration of a sample into account; 100% concentration means that all of the "extra" molecules within a fluid sample are of one species.

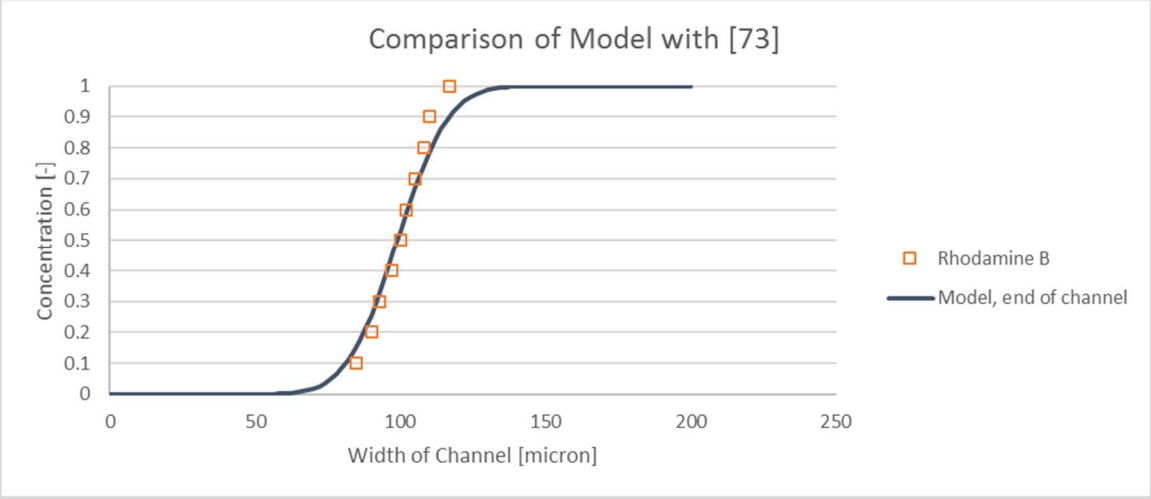

Figure 27. Comparison of Rhodamine B from van Leeuwen et al. [73] and modeling.

At its best fit, the profile of the model in Figure 27 shows an agreement of within 5% of van Leeuwen et al. [73]. The data does stray up to 40% nearing a nominal concentration of 1.

Experimental validation:

The diffusion channel begins after the two inlets combine. Each inlet is a 300-micron square; therefore, the diffusion channel is 600 microns wide with a depth of 300 microns. The inlet channels can be as long as needed prior to making a 90° turn into the diffusion channel. In experimental setup, the lengths were 2 cm. The flow rate is set and controlled by a KD Scientific Legato 180 syringe pump for laboratory verification rather than by hand. Flow rates are kept under 100 microliters per minute to allow the Reynolds number to stay at a value under 5. For modeling purposes, it is assumed the flow has already made its initial 90° corner into the channel before the length is measured.

The exact solution is solved for as shown below in Figure 28. This representation of the error function is compared with experimental data collected in lab with fluorescing beads suspended in water. A video microscope measured and recorded optical intensity from its viewer.

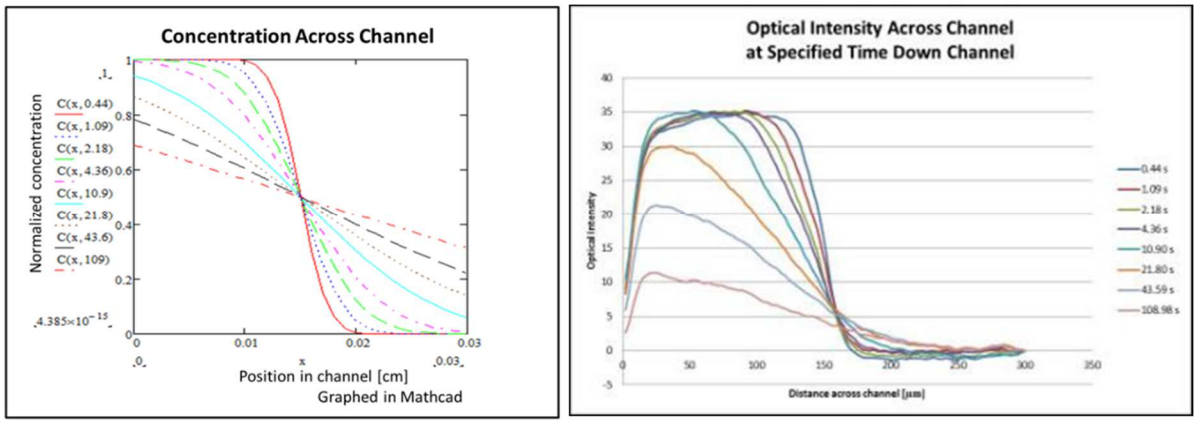

Figure 28. Results of modeling on the left. Actual optical measurements on the right [81].

Figure 28 shows a collapsed side between 150–300 μm where all reported intensities are at 0 and the centerline is not at half as numerically expected. This inconsistency was mentioned previously. It is speculated that light fixtures shining onto the channels to illuminate the

beads caused shadows that were picked up by the analysis software. Likewise, photobleaching could have caused the unnatural centerline data where the light was too bright to distinguish any details. This points out the need for fluorophores; they give off a different wavelength of light than the lights in a laboratory or sunlight, and perhaps even the sunlight that is filtered through Mars atmosphere.

What needs to be incorporated now is the use of small particles on a continuum basis and the movement of concentrations between the two fluids. For this particular flow problem, a syringe pump controls the flow rate through the microchannel. This can range from 0.1–100 μL/min depending on the user-controlled settings.

Unpublished results from experimental work includes Figure 29 where two fluids are flowing into the H-filter. This happened to be water for both inlet streams that contained an organic food dye to distinguish each side.

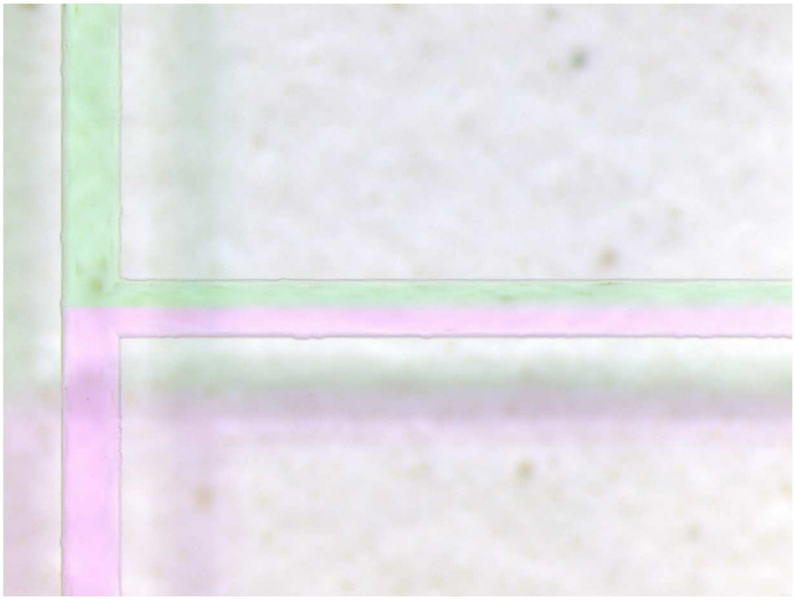

Figure 29. Experimental results for water-water with organic food dye [82].

The inlet also shows shadowing effects and defects in the walls. Etching should be more precise than what is presented here but raises awareness that chemical etching into borofloat glass wafers can include unexpected imperfections. Once again, the lighting issue could be filtered out if the fluorescence was a different wavelength that the camera could filter rather than at a wavelength the human eye can detect.

The details of Figure 30 are showing how water and isopropyl alcohol (IPA) interact within the diffusion channel in comparison to dyed water streams. The diffusion coefficient of the dye was estimated to be $5x10^{-6}$ cm^2/s in water. Thermophysical properties were calculated for water and isopropanol at room temperature and a flow rate of 10 μL/min. The diffusion coefficient of the food dye in the isopropanol was calculated to be $1.9x10^{-8}$ cm^2/s using an equivalent size for the dye molecule.

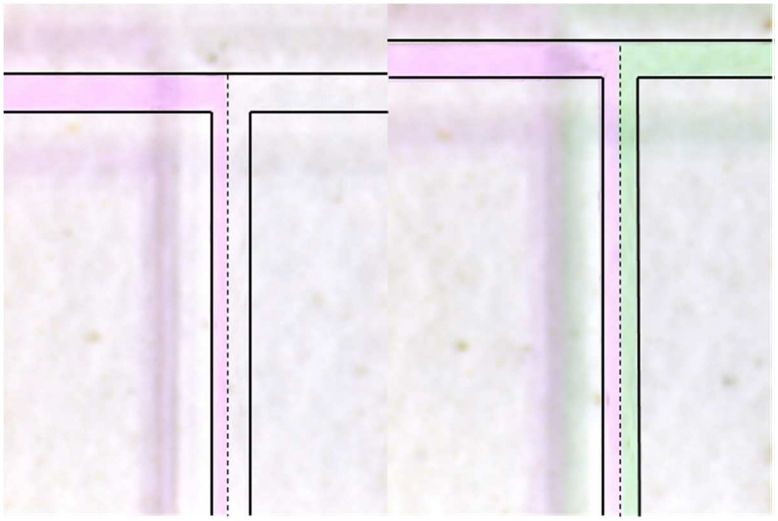

Figure 30. IPA-water, left, and water-water, right, to show what the optical capabilities of the system are [82].

The shadowing is very evident in these photographs, and the channels were outlined in post processing so that the edges could be distinguished from the rest of the material substrate. A raw image in Figure 31 demonstrates how the camera was moved during the experiment to

capture both inlet and outlet ends of the diffusion channel. The pink dye does begin to blend with the green side.

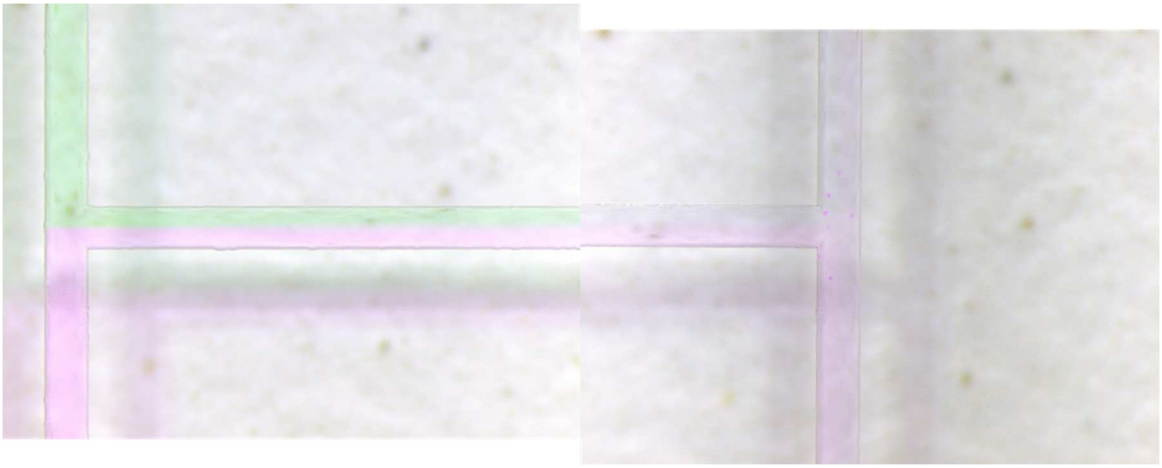

Figure 31. Water-water system with food coloring at 1 microliter per minute [82].

Figure 32 is the same setup as Figure 31 except the flow rate is increased tenfold. When the images are compared side-by-side, the diffusion of the dyes is evident in Figure 31, whereas in Figure 32, the streams are separate but some of the red dye exits with the green dye.

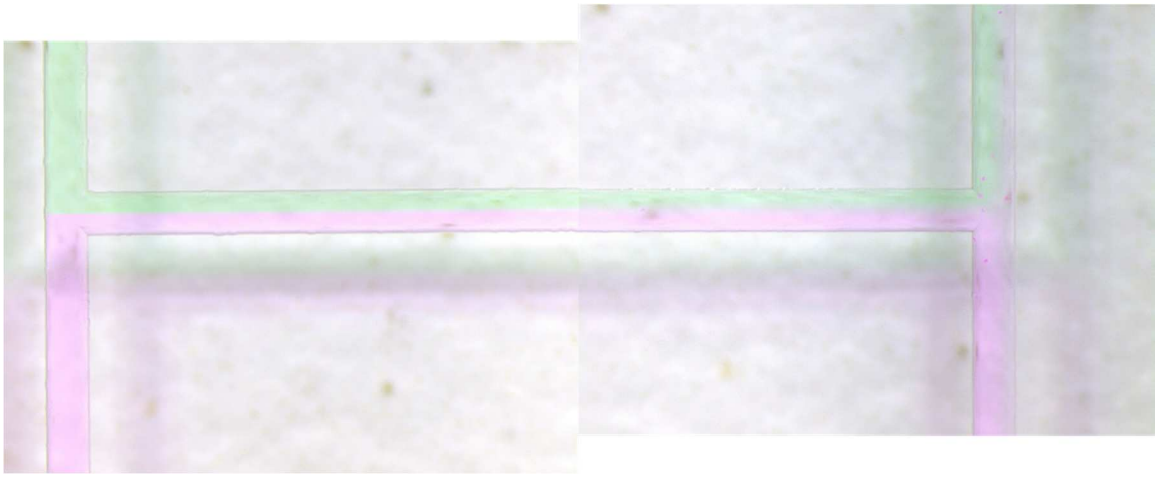

Figure 32. Water-water system with food coloring at 10 microliters per minute [82].

This serves as a demonstration for the flow keeping separate around corners while at a low enough Reynolds number, flow stream separation is possible.

Figures 31 and 32 are a water-water system. Figures 33 and 34 show an increase of flow rate but use IPA and water instead.

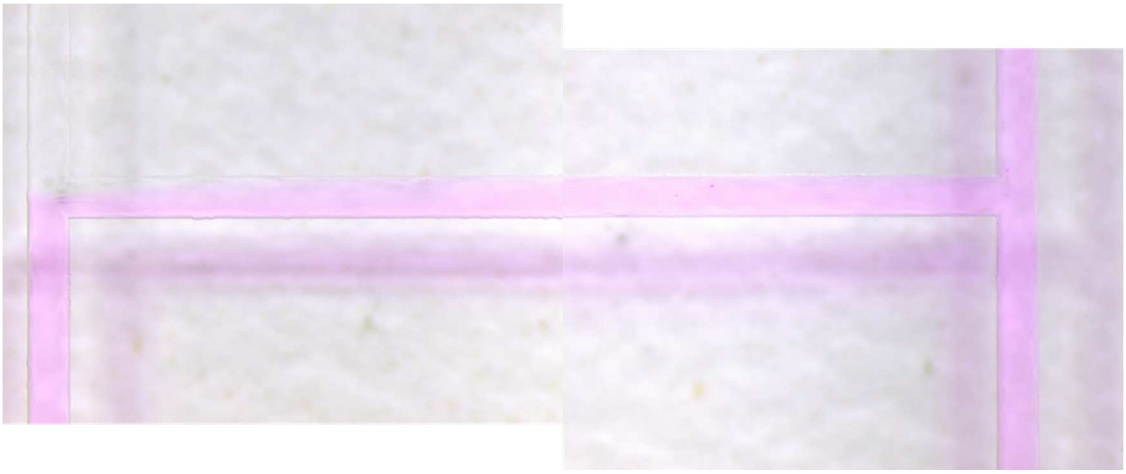

Figure 33. IPA-water with a flow rate of 1 microliter per minute [82]. The water is pink.

The setup in Figure 33 shows that the two streams either mix together or the dye diffuses completely by 2 mm into the length of the 2 cm diffusion channel. Figure 34 increases the flow rate by 50 times that of Figure 33.

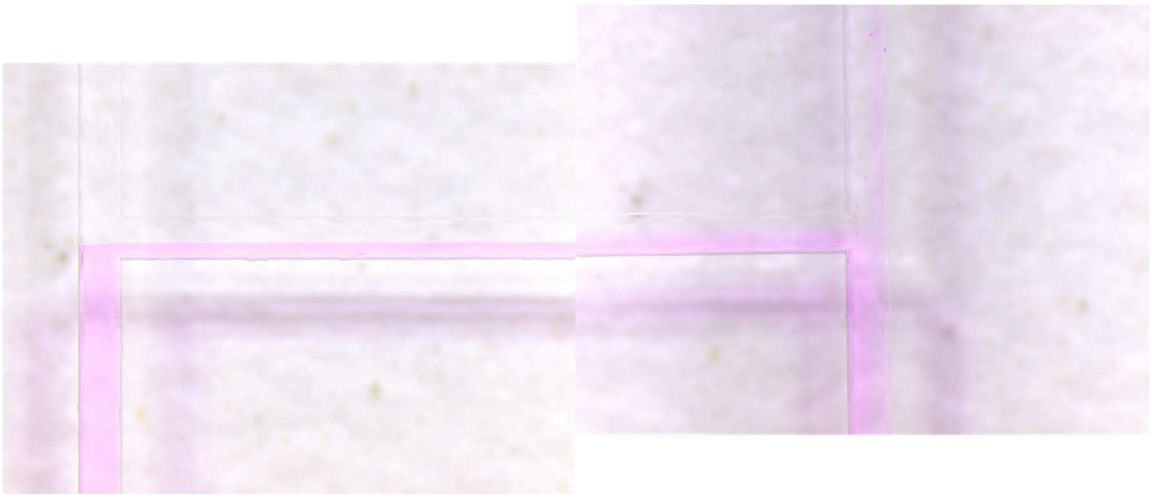

Figure 34. IPA-water with a flow rate of 50 microliters per minute [82]. The water is pink.

With the faster flow rate, the IPA and water keep separate. Some water has exited to the top right of the photo with the IPA, and not much of the food dye has diffused into the IPA.

The results of the experiments matched to results of modeling within 8% for the water-water system; the model predicts 1.88 mm for a 60%/40% concentration split (as opposed to 50% where everything is equally diffused and 100%/0% for the start of the channel). The pink stream takes over the diffusion channel at approximately 1.75 mm. The deviation may be due to the diffusion coefficient error.

The results of the IPA-water system differ greatly from the model (by 50%). The deviation from what the model predicted can be explained by the miscibility of the IPA with the water. This mixing was noticed most prominently with the slower flow rate.

Another test was to introduce bubbles into the lines. Though this was initially accidental, the bubble took up the entire width of the diffusion channel. As the bubble passed under the microscope, both streams experienced stopped flow. As the bubble left the viewing area, one stream took over the entire channel, then slowly retreated to the centerline where the LFDI of the fluid streams began to allow the second stream flow volume in the same channel. This balancing, or evenness, is because both streams were the same fluid moving at the same flow rate. As pointed out in Chapter 2, the viscosity difference and flow rate are proportional though this did not affect the bubble experiment. Further tests could use this incident to prove additional theories.

The experiments in the lab were done with the following equipment. Figure 35 shows the syringes with dyed fluid in them and computer-controlled flow rates.

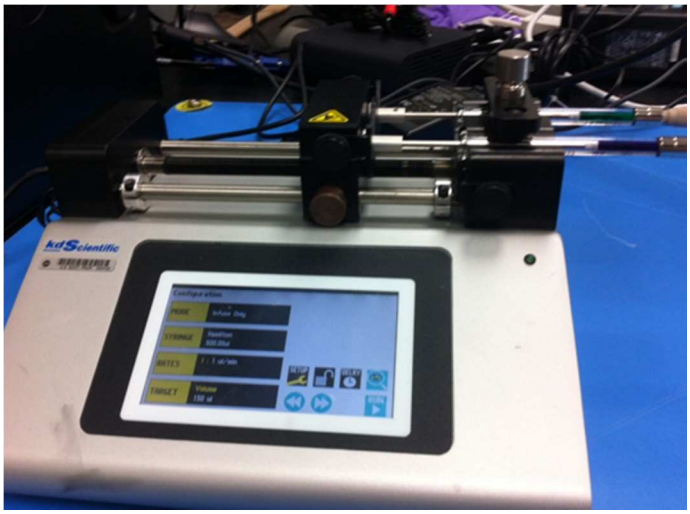

Figure 35. Syringe pump for experimental setup [83].

The syringe pump is not flight certified for traveling with the ABN. Each syringe can be individually controlled by the pump to allow a simulation with various flow rates. The consistency provided by a pump or electronic equipment is needed rather than gravity-fed lines or hand-forced syringes lacking reliability and the possibility of clogging. Figure 36 shows the lines leaving the syringes for the H-filter.

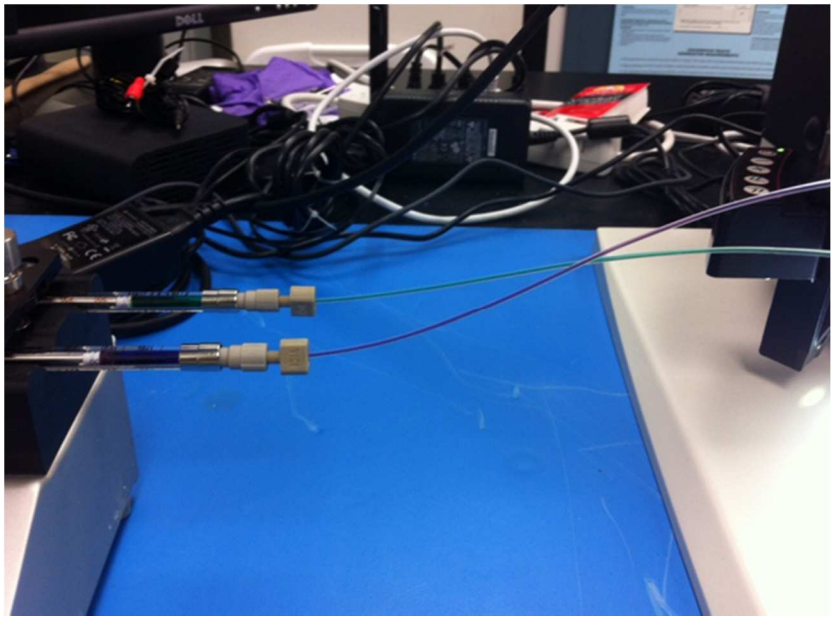

Figure 36. Input lines from syringe pump [83].

These lines carry water containing food coloring for visibility and to distinguish the fluid streams while inside the diffusion channel. The food coloring is not a reliable material as it has temperature dependence and will begin to break down above boiling at atmospheric pressures.

The experiment was tested with fluorospheres at a density of 1.06 kg/m^3 and a diameter of 4.8 microns. The beads are stirred in a beaker of water at 1% volume by weight before being drawn into the syringe for the pump. Figure 37 shows fluorescence of the channel as the water streams move through the channel. The bottom half of the channel contains the beads.

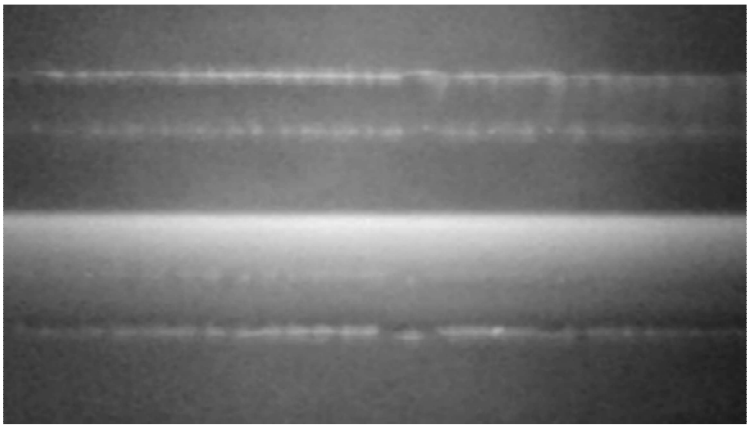

Figure 37. Fluorospheres in water. Second fluid is also water. LFDI brightest part of the channel (at centerline) [81].

The beads flow through the diffusion channel with a total flow rate of 100 μL/min. This is faster than the flow rates of the isopropanol/water and water/water experiments. Settling occurred at slower flow rates. Figure 37 also shows the channel wall shadow where improper lighting causes a “doubled” wall to appear. These artifacts show once again that etching does not result in smooth walls and workmanship should be inspected for rough walls that may result in eddy formation or cause a roughness factor to be incorporated into the calculations in place of smooth wall assumptions.

It was determined with the fluorescent beads that any concentration greater than 10% volume by weight would begin to settle in the syringe even before entering the diffusion channel. Settling was still a problem with 1% by weight if the flow rate was slow (less than 100 μL/min).

Chapter 6: Conclusion

Molecular species transfer within the microchannel between two different fluids is plausible and reliable. The use of partial differential equations with software modeling can predict the bulk fluid movement as well as the molecular diffusion. Resulting distances and times can be calculated based on the models with a 90% reliability.

When compared with experimental results performed alongside JPL colleagues, the predictions are within this 90% reliability. The missing link for a quantifiable result is the fluorescence detection (or count of molecules in the case of food dye) that make up the experimental validation section of Chapter 5. The comparison of the error function with early results as shown in Figure 28 worked because of the software program of a microscope that quantified the "brightness" of a sample. This quantification was not always reliable and changed with the lighting scenario in the laboratory.

The model is compared to literature results. In the example of [34], the molecular concentration does make a difference in the results. This molecular concentration is not a consideration in the model though it would affect the reaction rate and ability of the molecules in the fluid streams to find and react with each other.

As far as the occurrence of temperature effects, the temperature changes from the SCWE process may cause the acetone to vaporize inside the diffusion channel if the water is warmer than the vapor pressure of the acetone. If cooling is allowed before the water reached the diffusion channel, this would not be a concern. If another fluid with a vapor pressure similar to the vapor pressure of water is used as a fluorescing agent carrier instead of the acetone, this would also alleviate any concern of empty channels due to vaporization

of the carrier fluid. Temperature also changes the diffusion coefficients by over 100% increase or decrease from an average ("room") temperature.

The Reynolds numbers of the fluids are low enough that flowing two fluids through a microchannel without the fluids mixing is possible. It is also possible to allow diffusion between the streams. Through geometric design during the manufacturing of the microchannel network, specific lengths and outlet schemes can help to control how much of each fluid is collected or separated.

The experimental results compare well to the calculated results if diffusion coefficients are accurate. A difference in temperature or molecular size can have a significant impact on the model results (+/- 10% error) due to the diffusion coefficient influence in the resulting calculation.

Fluorescamine is modeled through the diffusion channel at a rate of 1 μL/min and 10 μL/min. The diffusion of fluorescamine places the molecule reacted with an amino acid into the acetone stream by 0.3 mm. The most reliable use of the diffusion channel is to allow products of the fluorescamine-amino acid reaction to migrate to the acetone side. Since fluorescamine can also fluoresce due to a reaction with water, the strength of the "glow" on the water side may be unfairly influenced by these fluorescamine-water products. Diffusion to the acetone side will take longer because the molecules and products diffuse faster through water.

No calculations or predictions are made for equating the fluorescence strength to the concentration of the molecules in either fluid along the diffusion channel. With a scanning optics device, moving only half the width of the channel would speed the data collection and allow for a more accurate measurement of fluorescence strength. The best position to place

the optics would be at this 1.88 mm location where most of the diffusion has taken place. It also is advisable to take optics measurements while the fluid is flowing at the faster flow rate; this allows for greater spacing between concentrations and avoids measurements during stopped flow conditions.

Chapter 7: Future Work

This work can be improved by using diffusion coefficients that are temperature dependent. Not many chemicals have data for their diffusion coefficients for more than one state point, which is most commonly room temperature at atmospheric pressure. Since some of these references include mentions of using microfluidic devices as a way to measure the diffusion coefficient for a chemical or fluid, it is possible at some point in time, precise measurements of the diffusion coefficient should be incorporated. If the channel can be heated to a steady and consistent temperature for the length of the channel, it would be possible to measure the diffusion coefficient for a range of temperatures. An equation describing the dependence on temperature by this coefficient could be made to improve Equation 7.

Additional work to the coefficients of diffusion and friction would be helpful to describe the model completely. As new technologies on micro- and nanoscales emerge, material descriptions will need to be confirmed based on the processing in clean rooms and the accuracy of etching “smooth-walled” channels. Theoretically, the channels should be completely smooth. As evident in some of the photos from the experiments, that was not always the case. A bad batch of etching chemicals or a mask that was not printed and laid on the chip cleanly could have caused some of these geometric inconsistencies. One suggested improvement for future etching is to round the sharp corners at the entrance turn from the inlet to the diffusion channel. Though this portion of the channel was not investigated, making the 90° direction change would allow for a smoother direction change for the fluid and prevent eddy formation if the corner was not as blunt.

Different fluid carriers would provide a broader temperature range than the limits set by the vapor pressures of acetone and water. This is prevented currently with a cooldown period after the water is processed through the SCWE portion of the system.

The design can be improved overall by incorporating an active and passive system to allow larger particles to pass through the H-filter. An active system may be a visual feedback loop to increase flow rates to allow less time for particles to settle. A passive system may include geometry changes to cause eddies that kick up sinking particles into the middle of the flow channel.

Other families of fluorescing agents might be better since fluorescamine has such a high affinity of binding with water. This is currently overcome by focusing detection on the acetone side of the channel, but there may be another chemical less reactive in combination with another particle-carrying fluid instead of water. Acetone and water systems could be exchanged for fluids that are less polar and can stay within the limits of the vapor pressure much easier than the limited range of temperatures in which these fluids must operate. Even with the low freezing point of acetone, it still must contest with its relatively low vapor pressure compared to water at the same temperature.

It may be possible to have a third fluid sandwiched and flowing in the diffusion channel that is incorporated as a buffer which fluorescamine and amino acids move into from the acetone and water as the outermost fluids in the channel. That way, fluorescamine has a buffer between it and water molecules, and the binding reaction between fluorescamine and amino acids can happen in a neutral location.

The results compared with the experimental work of isopropanol and water show a discrepancy between predicted and actual diffusion. The affinity and solubility

characteristics between isopropanol and water should be investigated further to fully understand the mechanisms between two reactive streams of fluid. This would provide an informed decision for the selection of carrier fluids for both the sample and the reacting streams.

One topic not investigated in this work that may be useful in the future is how far heating and cooling carry through the material substrate from the SCWE portion of the chip to the diffusion channel. ANSYS may be capable of incorporating heat transfer in a solid material that surrounds the moving liquid, but that is not investigated in this body of work. Ice plug timing and thermal cycling are not covered either but these effects, along with a model to specifically address heat transfer from the walls and throughout the moving fluid would add to the understanding of the entirety of transport phenomena in microchannel design.

References

[1] NASA Astrobiology. https://astrobiology.nasa.gov

[2] https://astrobiology.nasa.gov/astep/projects/nra/nnh10zda001n-astid/astrobionibbler-integrated-macroscopic-sample-acqu/

[3] The International Association for the Properties of Water and Steam (IAPWS). 1995 Formulation for the Thermodynamic Properties of Ordinary Water Substance for General and Scientific Use (1995).

[4] M. Lee and A. Noell. Unpublished experiment performed at the Jet Propulsion Laboratory/Caltech (2013).

[5] M. Lee. Unpublished experimental setup at the Jet Propulsion Laboratory/Caltech (2012).

[6] M. Holl, P. Galambos, F. Forster, J. Brody and P. Yager. Optimal Design of a Microfabricated Diffusion-based Extraction Device. *Proceedings of 1996 ASME Meeting.* ASME DSC59, 189-195 (1996).

[7] J. Brody, T. Osborn, F. Forster and P. Yager. A Planar Microfabricated Fluid Filter. *Sensors and Actuators A*. 54, 704-708 (1996).

[8] E. Hausler, P. Domagalski, M. Ottens, and A. Bardow. Microfluidic Diffusion Measurements: The Optimal H-cell. *Chem. Engr. Sci.* 72, 45 (2012).

[9] E. Livak-Dahl, I. Sinn and M. Burns. Microfluidic Chemical Analysis Systems. *Annu. Rev. Chem. Biomol. Eng.* 2, 325-53 (2011).

[10] J. Brody, A. Kamholz, and P. Yager. Prominent Microscopic Effects in Microfabricated Fluidic Analysis Systems. *SPIE*. 2978, 103-110 (1997).

[11] E. Purcell. Life at Low Reynolds Number. *American Journal of Physics*. 45, 3-11 (1977).

[12] J. Brody, P. Yager, R. Goldstein and R. Austin. Biotechnology at Low Reynolds Numbers. *Biophysical Journal*. 71, 3430-3441 (1996).

[13] J. Adeosun and A. Lawal. Mass Transfer Enhancement in Microchannel Reactors by Reorientation of Fluid Interfaces and Stretching. *Sensors and Actuators B.* 110, 101-111 (2005).

[14] V. Mengeaud, J. Josserand and H. Girault. Mixing Processes in a Zigzag Microchannel: Finite Element Simulations and Optical Study. *Anal. Chem.* 74, 4279-4286 (2002).

[15] R. Bird, W. Stewart and E. Lightfoot. Transport Phenomena, Second Edition. Wiley (2007).

[16] J. Li and Y. Renardy. Numerical Study of Flows of Two Immiscible Liquids at Low Reynolds Numbers. *SIAM Review*. 42, 417-439 (2000).

[17] B. Finlayson. Poiseuille Flow of Two Immiscible Fluids Between Flat Plates with Applications to Microfluidics. (2010).

[18] P. Williams, S. Levin, T. Lenczycki and J. Giddings. Continuous SPLITT Fractionation Based on a Diffusion Mechanism. *Ind. Eng. Chem. Res*. 31, 2172-2181 (1992).

[19] B. Schattka, M. Alexander, S. Low-Ying, A. Man and R. Shaw. Metabolic Fingerprinting of Biofluids by Infrared Spectroscopy: Modeling and Optimization of Flow Rates for Laminar Fluid Diffusion Interface Sample Preconditioning. *Anal. Chem.* 83, 555-562 (2011).

[20] C. Mansfield, A. Man, S. Low-Ying and R. Shaw. Laminar Fluid Diffusion Interface Preconditioning of Serum and Urine for Reagent-Free Infrared Clinical Analysis and Diagnostics. *Applied Spectroscopy*. 59, 10-15 (2005).

[21] P. Jandik, B. Weigl, N. Kessler, J. Cheng, C. Morris, T. Schulte and N. Avdalovic. Initial Study of Using a Laminar Fluid Diffusion Interface for Sample Preparation in High-Performance Liquid Chromatography. *Journal of Chromatography A*. 954, 33-40 (2002).

[22] K. Nelson, J. Foley and P. Yager. Concentration Gradient Immunoassay. 1. An Immunoassay Based on Interdiffusion and Surface Binding in a Microchannel. *Anal. Chem.* 79, 3542-3548 (2007).

[23] J. Foley, K. Nelson, A. Mashadi-Hossein, B. Finlayson and P. Yager. Concentration Gradient Immunoassay. 2. Computational Modeling for Analysis and Optimization. *Anal. Chem*. 79, 3549-3553 (2007).

[24] J. Kuo and D. Chiu. Controlling Mass Transport in Microfluidic Devices. *Annu. Rev. Anal. Chem*. 4, 275-96 (2011).

[25] A. Hatch, E. Garcia and P. Yager. Diffusion-based Analysis of Molecular Interactions in Microfluidic Devices, *Proceedings of the IEEE.* 92, 126 (2004).

[26] B. Kuczenski, P. LeDuc and W. Messner. Pressure-Driven Spatiotemporal Control of the Laminar Flow Interface in a Microfluidic Network. *Lab Chip.* 7, 647-649 (2007).

[27] B. Poling, J. Prausnitz and J. O'Connell. The Properties of Gases and Liquids, Fifth Edition. McGraw Hill (2001).

[28] A. Kamholz and P. Yager. Molecular Diffusive Scaling Laws in Pressure-driven Microfluidic Channels: deviation from one-dimensional Einstein approximations. *Sensors and Actuators B.* 82, 117-121 (2002).

[29] S. Bowden, P. Monaghan, R. Wilson, J. Parnell and J. Cooper. The Liquid-Liquid Diffusive Extraction of Hydrocarbons from a North Sea Oil Using a Microfluidic Format. *Lab Chip*. 6, 740-743 (2006).

[30] R. Ismagilov, A. Stroock, P. Kenis, G. Whitesides and H. Stone. Experimental and Theoretical Scaling Laws for Transverse Diffusive Broadening in Two-Phase Laminar Flows in Microchannels. *Appl. Phys Lett.* 76, 2376-2378 (2000).

[31] M. Kashid, D. Agar and S. Turek. CFD Modelling of Mass Transfer with and without Chemical Reaction in the Liquid-Liquid Slug Flow Microreactor. *Chemical Engineering Science*. 62, 5102-5109 (2007).

[32] A. Kamholz and P. Yager. Theoretical Analysis of Molecular Diffusion in Pressure-Driven Laminar Flow in Microfluidic Channels. *Biophysical Journal.* 80, 155-160 (2001).

[33] B. Weigl and P. Yager. Microfluidic Diffusion-based Separation and Detection. *Science*. 283, 346-347 (1999).

[34] A. Kamholz, B. Weigl, B. Finlayson and P. Yager. Quantitative Analysis of Molecular Interaction in a Microfluidic Channel: The T-Sensor. *Anal. Chem.* 71, 5340-5347 (1999).

[35] H. Stone, A. Stroock and A. Ajdari. Engineering Flows in Small Devices: Microfluidics Toward Lab-on-a-Chip. *Annu. Rev. Fluid Mech.* 36, 381-411 (2004).

[36] A. Skelley, J. Scherer, A. Aubrey, W. Grover, R. Ivester, P. Ehrenfreund, F. Grunthaner, J. Bada and R. Mathies. Development and Evaluation of a Microdevice for Amino Acid Biomarker Detection and Analysis on Mars. *PNAS.* 102, 1041-1046 (2005).

[37] V. Kapoor, C. Jafvert and D. Lyn. Experimental Study of a Biomolecular Reaction in Poiseuille Flow. *Water Resources Research*. 34, 1997-2004 (1998).

[38] B. Weigl, R. Bardell, N. Kesler and C. Morris. Lab-on-a-chip Sample Preparation Using Laminar Fluid Diffusion Interfaces – Computational fluid dynamic model results and fluidic verification experiments. *J. Anal. Chem.* 371, 97-105 (2001).

[39] B. Weigl, G. Domingo, P. LaBarre and J. Gerlach. Towards Non- and Minimally Instrumented, Microfluidics-based Diagnostic Devices. *Lab Chip*. 8, 1999-2014 (2008).

[40] X. Mu, A. Liang, P. Hu, K. Ren, Y. Wang and G. Luo. Selectively Modified Microfluidic Chip for Solvent Extraction of Radix Salvia Miltiorrhiza Using Three-Phase Laminar Flow to Provide Double Liquid-Liquid Interface Area. *Microfluid Nanofluid.* 9, 365-373 (2010).

[41] C. Culbertson, S. Jacobson, J. Ramsey. Diffusion Coefficient Measurements in Microfluidic Devices. *Talanta.* 56, 365-373 (2002).

[42] E. Choban, L. Markoski, A. Wieckowski and P. Kenis. Microfluidic Fuel Cell Based on Laminar Flow. *Journal of Power Sources.* 128, 54-60 (2004).

[43] T. McKay. A CFD Model of Mixing in a Microfluidic Device for Space Medicine Technology. Dissertation – Cleveland State University (2003).

[44] C. Nonino, S. Savino and S. Del Giudice. Numerical Assessment of the Mixing Performance of Different Serpentine Microchannels. *Heat Transfer Engineering*. 30, 101-112 (2009).

[45] S. Jayanti, G. Hewitt and J. Kightley. Fluid Flow in Curved Ducts. *International Journal for Numerical Methods in Fluids.* 10, 569-589 (1990).

[46] C. Culbertson, S. Jacobson and J. Ramsey. Microchip Devices for High-Efficiency Separations. *Anal. Chem.* 72, 5814-5819 (2000).

[47] N. Solehati, J. Bae and A. Sasmito. Numerical Investigation of Mixing Performance in Microchannel T-junction with Wavy Structure. *Computers & Fluids.* 96, 10-19 (2014).

[48] P. Tabeling. A Brief Introduction to Slippage, Droplets and Mixing in Microfluidic Systems. *Lab Chip.* 9, 2428-2436 (2009).

[49] C. Pozrikidis. Motion of a Spherical Particle in Film Flow. *J. Fluid Mech.* 566, 465-475 (2006).

[50] J. Brody and P. Yager. Diffusion-based Extraction in a Microfabricated Device. *Sensors and Actuators A*. 58, 13-18 (1997).

[51] C. Priest, J. Zhou, R. Sedev, J. Ralston, A. Aota, K. Mawatari, and T. Kitamori. Microfluidic Extraction of Copper from Particle-laden Solutions. *International Journal of Mineral Processing.* 98, 168-173 (2011).

[52] C. Priest, J. Zhou, S. Klink, R. Sedev, and J. Ralston. Microfluidic Solvent Extraction of Metal Ions and Complexes from Leach Solutions Containing Nanoparticles. *Chemical Engineering Technologies*. 35, 1312-1319 (2012).

[53] S. Chen and S. Jiang. Determination of Cadmium, Mercury and Lead in Soil Samples by Slurry Sampling Electrothermal Vaporization Inductively Coupled Plasma Mass Spectrometry. *J. Anal. At. Spectrom*. 13, 1113-1117 (1998).

[54] M. Cal-Prieto, A. Carlosena, J. Andrade, S. Muniategui, P. Lopez-Mahia, E. Fernandez and D. Prada. Development of an Analytical Scheme for the Direct Determination of Antimony in Geological Materials by Automated Ultrasonic Slurry Sampling-ETAAS. *J. Anal. At. Spectrom.* 14, 703-710 (1999).

[55] X. Amashukeli, C. Pelletier, J. Kirby, and F. Grunthaner. Subcritical Water Extraction of Amino Acids from Atacama Desert Soils. *J. Geophys. Res.* 112, 1 (2007).

[56] C. Malmberg and A. Maryott. Dielectric Constant of Water from 0° to 100°C. *Journal of Research of the National Bureau of Standards.* 56, 1 (1956).

[57] X. Amashukeli, F. Grunthaner, S. Patrick, and P. To Yung. Subcritical Water Extractor for Mars Analog Soil Analysis. *Astrobiology.* **8**, 597 (2008).

[58] B. Xu, Ooti K. T., Wong N. T., and Choi W. K. Experimental Investigation of Flow Friction for Liquid Flow in Microchannels. *Int. Comm. Heat Mass Transfer*. 27, 1165-1176 (2000).

[59] W. Urbanek, J. Zemel and H. Bau. An Investigation of the Temperature Dependence of Poiseuille Numbers in Microchannel Flow. *J. Micromach. Microeng.* 3, 205-208 (1983).

[60] R. Bostic, S. Gunakala and S. Baragada. Heat Transfer in Adjacent Flow of Two Immiscible Fluids Bounded by Two Parallel Porous Beds – Darcy Model. *IJAIEM*. 2, 158-168 (2013).

[61] J. Avsec, G. Naterer and M. Oblak. Fluid Flow with Thermophysical Property Variations in Long Rectangular Minichannels and Microchannels. *AIAA/ASME Joint Thermophysics and Heat Transfer Conference*. 900-914 (2006).

[62] P. Wibulawas. Laminar-Flow Heat-Transfer in Non-Circular Ducts. Thesis. University College London. (1966).

[63] A. Kamholz, Schilling, and P. Yager. Optical Measurement of Transverse Molecular Diffusion in a Microchannel. *Biophysical Journal*. 80, 1967-1972 (2001).

[64] S. Udenfriend, S. Stein, P. Bohlen, W. Dairman, W. Leimgruber, and M. Weigele. Fluorescamine: A Reagent for Assay of Amino Acids, Peptides, Proteins, and Primary Amines in the Picomole Range. *Science.* 178 (1972).

[65] A. Skelley and R. Mathies. Chiral Separation of Fluorescamine-labeled Amino Acids Using Microfabricated Capillary Electrophoresis Devices for Extraterrestrial Exploration. *J. Chromatography A.* 1021, 191-199 (2003).

[66] T. Chiesl, W. Chu, A. Stockton, X. Amashukeli, F. Grunthaner and R. Mathies. Enhanced Amine and Amino Acid Analysis Using Pacific Blue and the Mars Organic Analyzer Microchip Capillary Electrophoresis System. *Anal. Chem.* 81, 2537-2544 (2009).

[67] P. Jandik, J. Cheng, D. Jensen, S. Manz and N. Avdalovic. Simplified In-line Sample Preparation for Amino Acid Analysis in Carbohydrate Containing Samples. *J. Chromatogr. B*. 758, 189-196 (2001).

[68] D. Beebe, G. Mensing and G. Walker. Physics and Applications of Microfluidics in Biology. *Annu. Rev. Biomed. Eng.* 4, 261-286 (2002).

[69] A. Hatch, A. Kamholz, K. Hawkins, M. Munson, E. Schilling, B. Weigl, and P. Yager. A Rapid Diffusion Immunoassay in a T-sensor. *Nat. Biotechnol.* 19, 461-465 (2001).

[70] M. Mora, A. Stockton and P. Willis. Microchip Capillary Electrophoresis Instrumentation for In Situ Analysis in the Search for Extraterrestrial Life. *Electrophoresis*. 33, 2624-2638 (2012).

[71] A. Skelley, J. Cleaves, C. Jayarajah, J. Bada and R. Mathies. Application of the Mars Organic Analyzer to Nucleobase and Amine Biomarker Detection. *Astrobiology*. 6, 824-837 (2006).

[72] I. Kate, J. Garry, Z. Peeters, R. Quinn, B. Foing and P. Ehrenfreund. Amino Acid Photostability on the Martian Surface. *Meteoritics and Planetary Science.* 40, 1185-1193 (2005).

[73] M. van Leeuwen, X. Li, E. Krommenhoek, H. Gardeniers, M. Ottens, L. van der Wielen, J. Heijnen and W. van Gulik. Quantitative Determination of Glucose Transfer Between Cocurrent Laminar Water Streams in a H-Shaped Microchannel. *Biotechnol. Prog.* 25, 1826-32 (2009).

[74] M. Brust, C. Schaefer, R. Doerr, L. Pan, M. Garcia, P. Arratia and C. Wagner. Rheology of Human Blood Plasma: Viscoelastic Versus Newtonian Behavior. *PRL.* 110, 07805 (2013).

[75] Fluorescamine. PubChem. https://pubchem.ncbi.nlm.nih.gov

[76] Probes. Reagents for Analysis of Low Molecular Weight Amines. www.thermofisher.com

[77] P. Kenis, R. Ismagilov and G. Whitesides. Microfabrication Inside Capillaries Using Multiphase Laminar Flow Patterning. *Science*. 285, 83-85 (1999).

[78] A. Stockton, T. Chiesl, T. Lowenstein, X. Amashukeli, F. Grunthaner and R. Mathies. Capillary Electrophoresis Analysis of Organic Amines and Amino Acids in Saline and Acidic Samples Using the Mars Organic Analyzer. *Astrobiology.* 9, 823-831 (2009).

[79] E. Lemmon and R. Span. Short Fundamental Equations of State for 20 Industrial Fluids. *J. Chem. Eng. Data*. 51, 3, 785-850 (2006).

[80] T. Dertinger, B. Ewers, I. Hocht and J. Enderlein. Dual-Focus Fluorescence Correlation Spectroscopy. Application Note PicoQuant (2011).

[81] A. Noell and J. Hasenoehrl. Unpublished experimental results performed at the Jet Propulsion Laboratory/Caltech (2013).

[82] M. Lee and A. Noell. Unpublished experimental results performed at the Jet Propulsion Laboratory/Caltech (2013).

[83] M. Lee. Unpublished experimental results performed at the Jet Propulsion Laboratory/Caltech (2013).

Bibliography

[1] Molecular Probes Handbook, ThermoFisher (2010).

[2] Perry's Chemical Handbook.

[3] K. Khanafer and K. Vafai. The Role of Nanoparticle Suspensions in Thermo/Fluid and Biomedical Applications. Nanoparticle Heat Transfer and Fluid Flow.

[4] J. Happel and H. Brenner. Low Reynolds Number Hydrodynamics (1983).

[5] H. Lomax, T. Pulliam and D. Zingg. Fundamentals of Computational Fluid Dynamics (2001).

[6] Thermo Fisher Scientific. Fluorescamine Protein Assay. Protocol. www.nanodrop.com

[7] H. Berg and E. Purcell. A Method for Separating According to Mass a Mixture of Macromolecules or Small Particles Suspended in a Fluid, I. Theory. *Physics.* 58, 862-869 (1967).

[8] H. Berg, E. Purcell and W. Stewart. A Method for Separating According to Mass a Mixture of Macromolecules or Small Particles Suspended in a Fluid, II. Experiments in a Gravitational Field. *Physics.* 58, 1286-1291 (1967).

[9] H. Berg and E. Purcell. A Method for Separating According to Mass a Mixture of Macromolecules or Small Particles Suspended in a Fluid, III. Experiments in a Centrifugal Field. *Physics.* 58, 1821-1828 (1967).

[10] R. Garesse, J. Castell, C. Vallejo and R. Marco. A Fluorescamine-Based Sensitive Method for the Assay of Proteinases, Capable of Detecting the Initial Cleavage Steps of a Protein. *Eur. J. Biochem.* 99, 253-259 (1979).

[11] B. Weigl, R. Bardell, and C. Cabrera. Lab-on-a-chip for Drug Development. *Advanced Drug Delivery Reviews.* 55, 349 (2003).

[12] P. Yager. Cutting Edge: A pre-filled, ready-to-use electrophoresis based lab-on-a-chip device for monitoring lithium in blood. *Lab Chip*. 10, 1757 (2010).

[13] G. Taylor. Film notes for Low-Reynolds-Number Flows. Education Development Center (1967).

[14] A. Balasubramanian, K. Soni, A. Beskok and S. Pillai. A Microfluidic Device for Continuous Capture and Concentration of Microorganisms from Potable Water. *Lab Chip*. 7, 1315-1321 (2007).

[15] H. Lee and J. Kim. Two-Dimensional Kelvin-Helmholtz Instabilities of Multi-Component Fluids. *European Journal of Mechanics B/Fluids*. 49, 77-88 (2015).

[16] M. Spiga and G. Morini. A Symmetric Solution for Velocity Profile in Laminar Flow Through Rectangular Ducts. *International Communications in Heat and Mass Transfer.* 21, 469-475 (1994).

[17] F. Guillen-Gonzalez and G. Tierra. Splitting Schemes for a Navier-Stokes-Hilliard Model for Two Fluids with Different Densities. *Journal of Computational Mathematics.* 32, 643-664 (2014).

[18] J. Yoo. Recent Studies on Fluid Flow and Heat Transfer in Thermal Microdevices. *Nanoscale and Microscale Thermophysical Engineering.* 10, 67-81 (2006).

[19] C. Wang, N. Nguyen, T. Wong, Z. Wu, C. Yang and K. Ooi. Investigation of Active Interface Control of Pressure Driven Two-Fluid Flow in Microchannels. *Sensors and Actuators A.* 133, 323-328 (2007).

[20] M. Hasenbank, E. Fu, J. Nelson, D. Schwartz and P. Yager. Investigation of Heterogeneous Electrochemical Processes Using Multi-Stream Laminar Flow in a Microchannel. *Lab Chip.* 7, 441-447 (2007).

[21] J. Lai, K. Nelson, M. Nash, A. Hoffman, P. Yager and P. Stayton. Dynamic Bioprocessing and Microfluidic Transport Control with Smart Magnetic Nanoparticles in Laminar-Flow Devices. *Lab Chip.* 9, 1997-2002 (2009).

[22] G. Zhang, M. Li, J. Li, M. Yu, M. Qi and Z. Bai. Wall Effects on Spheres Settling Through Non-Newtonian Fluid Media in Cylindrical Tubes. *J. of Dispersion Science and Technology.* 36, 1199-1207 (2015).

[23] G. Yohannes, S. Wiedmer, M. Elomaa, M. Jussila, V. Aseyev and M. Riekkola. Thermal Aggregation of Bovine Serum Albumin Studied by Asymmetrical Flow Field-Flow Fractionation. *Analytica Chimica Acta.* 65, 191-198 (2010).

[24] A. Chwang and T. Wu. Hydromechanics of Low-Reynolds-Number Flow. Part 2: Singularity method for Stokes Flow. *J. Fluid Mech.* 67, 787-815 (1975).

[25] J. Strikwerda. Finite Difference Methods for Stokes and Navier-Stokes Equations. *Technical Summary Report*. 2361 (1982).

[26] C. Jen, C. Wu, Y. Lin and C. Wu. Design and Simulation of the Micromixer with Chaotic Advection in Twisted Microchannels. *Lab Chip*. 2, 77-81 (2003).

[27] D. Capone, R. Popa, B. Flood and K. Nealson. Follow the Nitrogen. *Science.* 312, 708 (2006).

[28] Z. Wang, D. Tang, and X. Hu. Similarity Solutions for Flows and Heat Transfer in Microchannels Between Two Parallel Plates. *International Journal of Heat and Mass Transfer.* 54, 2349-2354 (2011).

[29] A. Stockton, C. Tjin, T. Chiesl and R. Mathies. Analysis of Carbonaceous Biomarkers with the Mars Organic Analyzer Microchip Capillary Electrophoresis System: Carboxylic Acids. *Astrobiology.* 11, 519-528 (2011).

[30] C. Nonino, S. Del Giudice, and S. Savino. Temperature-Dependent Viscosity and Viscous Dissipation Effects in Microchannel Flows with Uniform Wall Heat Flux. *Heat Transfer Engineering.* 31, 682-691 (2010).

[31] S. Del Giudice, C. Nonino, and S. Savino. Effects of Viscous Dissipation and Temperature Dependent Viscosity in Thermally and Simultaneously Developing Laminar Flows in Microchannels. *Int. J. Heat Fluid Flow.* 28, 15-27 (2007).

[32] L. Song and M. Elimelech. Particle Deposition onto a Permeable Surface in Laminar Flow. *J. Colloid Interface Sci.* 173, 165-180 (1995).

[33] H. Xiao, D. Liang, G. Liu, M. Guo, W. Xing and J. Cheng. Initial Study of Two-Phase Laminar Flow Extraction Chip for Sample Preparation for Gas Chromatography. *Lab Chip.* 6, 1067-1072 (2006).

[34] E. Wingender. Fluorescamine and Fluorescein; A New Energy-Transfer Pair and Its Application to the Binding of Histone H5 to Nucleosomes. *Analytical Biochemistry.* 121, 146-150 (1982).

Appendix A: Modeling

In order to add the bulk fluid flow, ANSYS Fluent used water and acetone in a single channel to calculate the velocity and pressure differences within the flow. Figure 38 shows the simulation of water entering bottom left, acetone entering top left, and the velocity vectors of the flow from the inlets to the outlets on the right side of the channel.

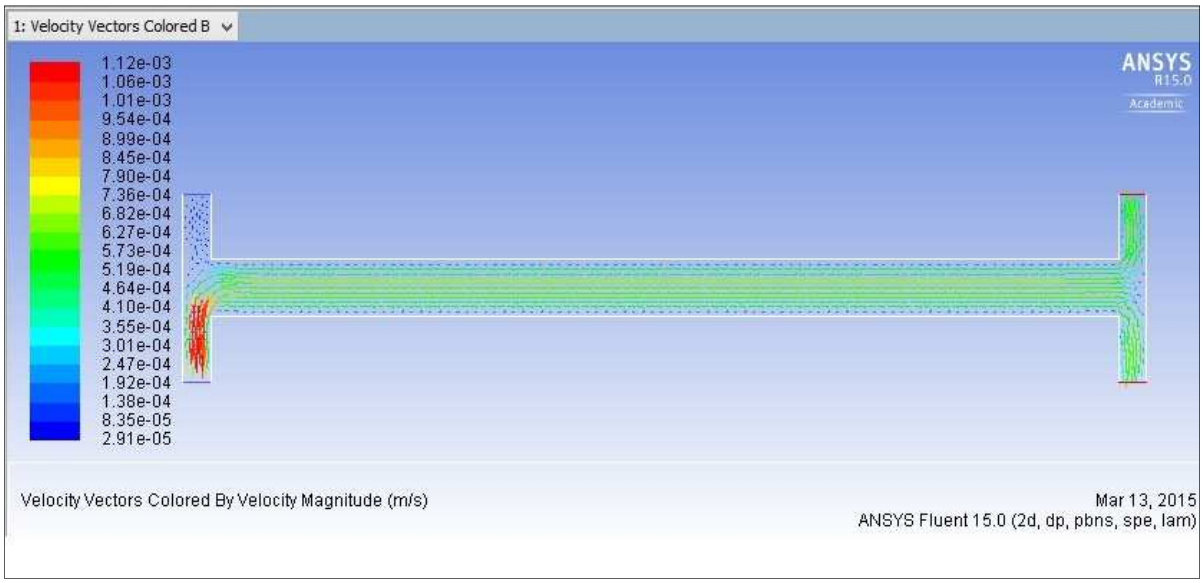

Figure 38. ANSYS Fluent simulation of two inlets, two outlets, and two fluids.

Adaptive meshing may be a possibility for the dual fluid approach while calculating the flow characteristics such as shear and velocities. An important reminder is that all of these calculated values are vector quantities, which means they cannot simply be added together like scalars. Each direction has a corresponding value, and only the z-direction was investigated for gravity effects. In reality, Mars has one-third the gravitational force as Earth, and it is possible the orientation of the wafers on a spacecraft may need to change. If the orientation changes, the gravitational force will need to be calculated for its effects on an additional direction.

The model uses finite differences whereas the CFD work uses Navier-Stokes equations for the momentum to solve the same conditions. The comparison between these two solutions should provide a relatively close match if the spatial and temporal steps are kept small and errors are not allowed to propagate. Boundary conditions are simulated with a solution that acts like a wall, or a zero flux boundary. These conditions are more difficult to solve for in MATLAB since the solution is set up to be a central difference solution in space.

Modeling what happens within the SCWE chamber helps determine what is happening with the heating and cooling on the chip, and it will help to predict the temperature at which the fluid entering the H-filter will be. This will affect the diffusion and chemical reaction times. The chamber is heated through a piezoelectric disc, which is seeded into the glass and is concentric with the chamber. The cooler is placed along the inlet and outlet channels to create an ice plug. The thickness of glass seems to be the largest influencer of whether the ice plugs hold. Experimental results suggest that the thickness and not the surface area in contact with the glass is the largest influence on the cooling power of the system and whether or not ice plugs will form and hold.

Appendix B: Comparison Data

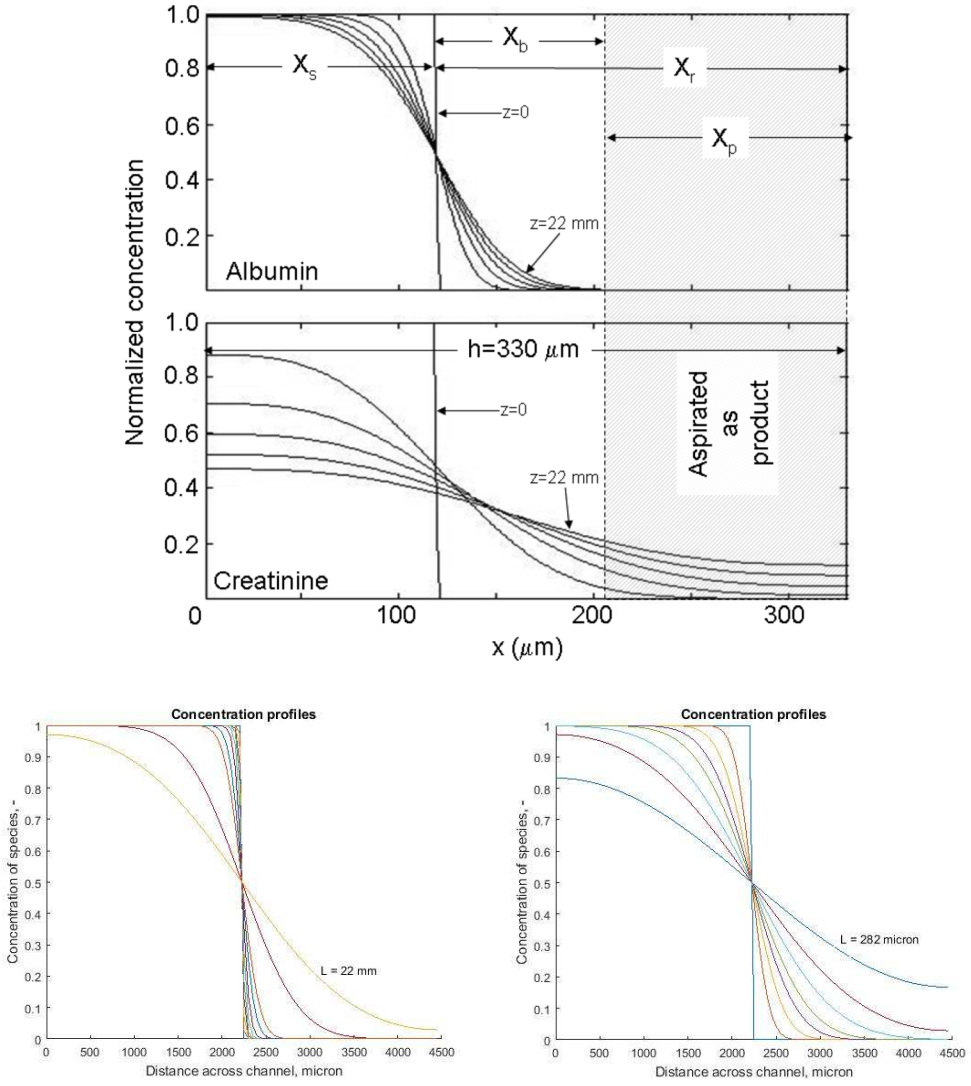

Figure 39. Albumin and creatinine diffusion profiles as presented by Schattka et al. [19].

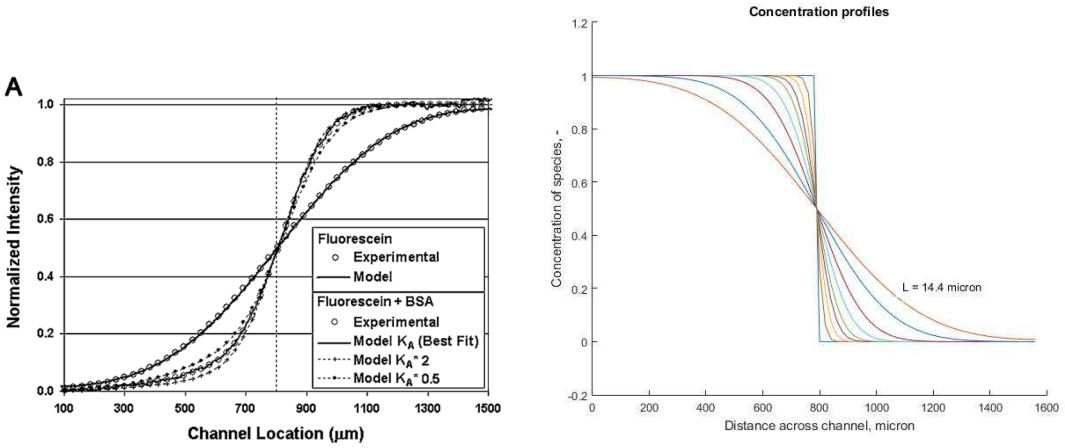

Figure 40. Fluorescein model and experimental results as presented by Hatch et al. [25].

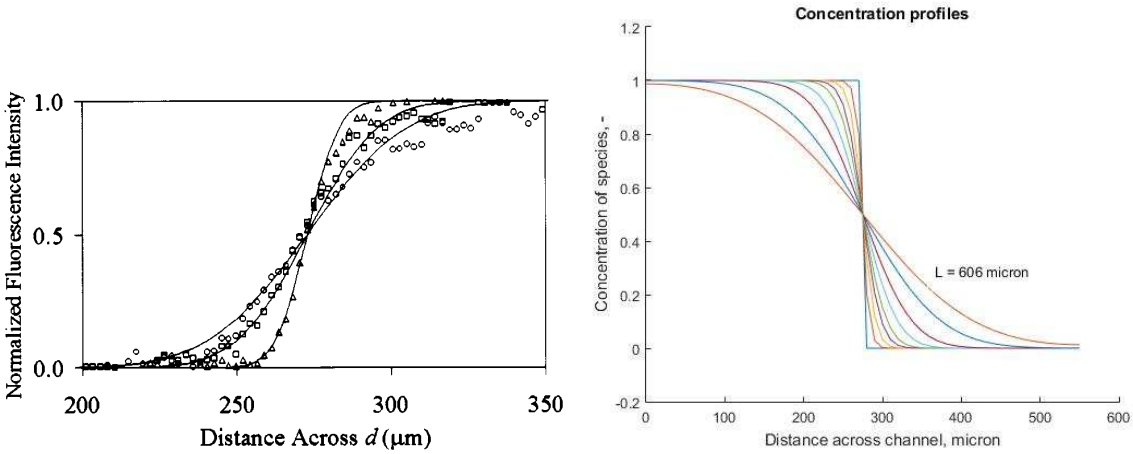

Figure 41. Results by Kamholz et al. [34].

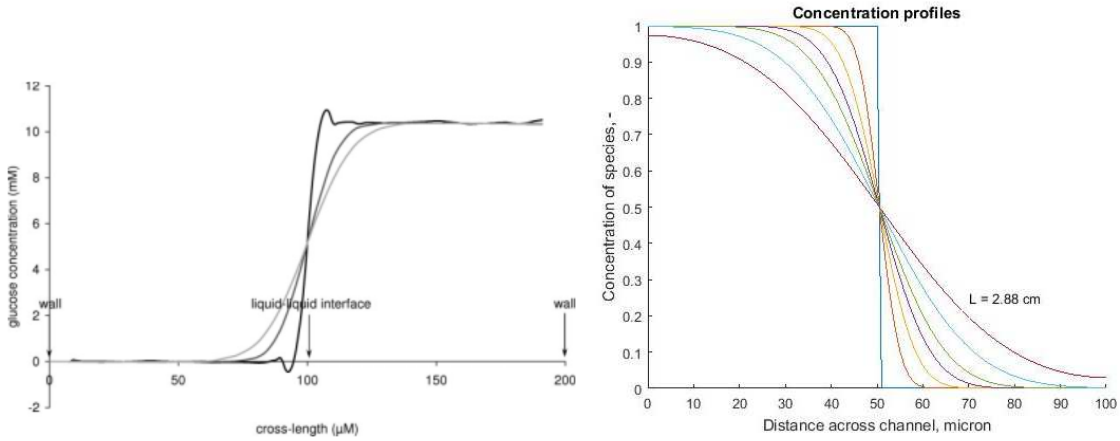

Figure 42. Rhodamine B concentration profile presented by van Leeuwen et al. [73].